DOI: 10.1002/ ((please add manuscript number))
Article type: Review

Body-Monitoring and Health Supervision by means of Optical Fiber-Based Sensing Systems in Medical Textiles

Brit M. Quandt, Lukas J. Scherer, Luciano F. Boesel, Martin Wolf, Gian-Luca Bona, René M. Rossi*

B. M. Quandt, Dr. L. F. Boesel, Dr. R. M. Rossi

Empa, Swiss Federal Laboratories for Materials Science and Technology, Laboratory for Protection and Physiology, Lerchenfeldstrasse 5, 9016 St. Gallen, Switzerland

* luciano.boesel@empa.ch

Prof. Dr. M. Wolf

Division of Neonatology, University Hospital Zurich, Frauenklinikstrasse 10, 8091 Zurich, Switzerland

Prof. Dr. G.-L. Bona

Empa, Swiss Federal Laboratories for Materials Science and Technology, Überlandstrasse 129, 8600 Dübendorf, Switzerland

Dr. L. J. Scherer

Radiometer Basel, Austrasse 25, 4051 Basel, Switzerland

Keywords:

fiber optic sensors, wearable systems, healthcare monitoring, smart textiles, long-term monitoring

---

Abstract

Long-term monitoring with optical fibers has moved into the focus of attention due to the applicability for medical measurements. Within this review, set-ups of flexible, unobtrusive body-monitoring systems based on optical fibers and the respective measured vital parameters are in focus. Optical principles are discussed as well as the interaction of light with tissue. Optical fiber-based sensors that were already used in first trials were primarily selected for the section on possible applications. These medical textiles included the supervision of respiration, cardiac output, blood pressure, blood flow and its saturation with hemoglobin as well as oxygen, pressure, shear stress, mobility, gait, temperature, and electrolyte balance. The implementation of these sensor concepts prompts the development of wearable smart textiles. Thus, current sensing techniques and possibilities within photonic textiles are reviewed leading to multi-parameter designs. Evaluation of these designs should show the great potential of optical fibers for the introduction into textiles especially due to the benefit of immunity to electromagnetic radiation. Still, further improvement of the signal to noise ratio is often necessary to develop a commercial monitoring system.

---

1. Introduction

Recent evaluations of the demographics of Western countries predict an increase in the number of elderly people from 11 to 22 % between 2000 and 2050. [1] In addition, it has been shown that frail people live longer in higher-income countries, indicating a benefit from more extensive healthcare. [2] While the number of medical treatments has increased and with it the share of the gross domestic product (GDP) for healthcare expenditures, the comfort and a high quality of life is expected as well. [3] The general preference and reduced cost of ambulant therapy combined with the societal changes lead to a search for new medical solutions.

From a medical point of view, a substantial demand for wearable monitoring systems for constant supervision (*e.g.* sudden death syndrome or cardiovascular diseases, type 2 diabetes) is present. Additionally, facilitation of a diagnostic decision is achieved with long-term monitoring systems. In contrast to snapshot analysis of fluctuating body parameters (*e.g.* blood sugar value, blood pressure, and heart rate), wearable systems for diagnostics promise continuous measurements throughout the day. [4] Potential users of wearable monitoring devices are not only the sick and rehabilitating, but also elite athletes for training purposes evaluating their progressing performance, profiting from portable therapeutic modules as well. [5] Recently, telemedicine has been in the focus of attention when remote diagnostics was used for sickened mountaineers. [6] In these situations, a measurement device transferring vital data can improve remote diagnostics and treatment plans.

For the resulting smart textiles, the production is essential – innovative techniques open new application areas and lead to measurement means with high reliability. Following the inclusion of the sensor components into the fabric, these systems require extensive software development. Additionally, the sensor communication across the body must allow for a normal range of motion and preserve comfort effectively as a physical state of ease without constraint. An autonomous life of the patient is the main goal and has to be maintained for ensuring a high quality of life. [7] These requirements on comfort set a high bar for the market introduction of new health supervision technologies. Furthermore, a reduction of the treatment costs is possible with textile body-monitoring systems. In-patients treatments are more expensive and use up much-needed hospital space.

Limiting the terms “intelligent system” and “wearable computing” to body-monitoring devices, not including therapeutic systems, it nevertheless includes many different types of devices, varying in communication degree. [8] An extensive list of wearable systems was compiled by Chan, Estève, Fourniols, Escriba, and Campo (2012). [3] Communication of the device ranges from a simpler visual output to a monitoring device to an evaluating diagnostic

signal. These can indicate a need for intervention to either patient or doctor. [9] Different approaches work on the management of biomedical information of a wireless body sensor network (WBSN). All of these lead towards supporting complex healthcare: They sense, diagnose and give feedback, resulting in therapeutic use. [10] However, the potential supervision can conflict with the ethics in surveillance as some systems include constant home supervision. Not only could health data be spread to unauthorized parties but the patients may prefer a less obtruded life over potential benefits. [3]

To conclude, unobtrusive systems documenting vital signs reliably in the patient's natural environment are preferential for managing and monitoring diseases. [8] Recent developments of these systems as well as existing commercial solutions have been documented, both in terms of sensing but also in transmitting the data. [10b, 11] Reported difficulties in building body-monitoring systems are the securing of contact quality, the occurrence of motion artifacts (body flab), muscle noise and patient comfort as well as the washability of the fabric. [12] Hence, a sensor-based approach will allow redesigning the measurement techniques of vital signs: First, defining the important parameters to a minimum degree of precision, followed by finding alternative approaches to fulfill these conditions, and then finally creating new systems including amplification, filtering, and transferring to a decision-making instance. [13] Smart textile fibers are reconsidered for traditionally electronics-based applications. [10b] These devices measure vital parameters reliably but are being redesigned for allowing omnipresent medical monitoring. The "light-in, light-out"-concept has generally become popular with recent discussions on the impact of radiation on the body and brain. [14] Methods to receive input on important body parameters by the means of light traveling through the body are thus advantageous. Additionally, the large surface of optical fibers invites for consideration of fiber surface sensors. [15] Current uses for optical fibers – both glass (GOF) and polymer (POF) – include communication purposes, structural health monitoring and more

recently also biomedical sensing. [16] Optical fibers also show great potential for usage in combination with other medical diagnostic machinery as they are immune to electromagnetic interference. [17] Furthermore, they are resilient to harsh environmental conditions and show high sensitivity. [18] While research on optical fibers started in the 1960s, further development in the production techniques for higher reliability has sparked renewed interest. [19]

This review is hence meant to serve as an introduction to the research developments of non-invasive body-monitoring with smart optical fibers. As smart fibers include many different materials, a separate research area has been established for the development of new optical fiber types. Therefore, optical fibers (OF), their operating principle and the resulting applications are separately introduced in **Section 2**. A special focus will lie on the possibilities for integration into textiles as an important condition to introduce smart textiles for medical applications. Optical fiber-based technologies will be compared with current alternative technologies. **Section 3** deals with the materials used for the production of optical fibers while **Section 4** focuses on the applications of these fibers. Wearable systems are finally discussed in **Section 5**. Concluding, **Section 6** wraps up the review and gives an outlook on future research and development.

2. Physics of light transmission in optical fibers and through human tissue

To understand the methods described in the subsequent sections, a basic understanding of the optical principles is needed. Hence this section serves as an introduction to fiber optics. The first subsection deals with light transmission and loss of optical fibers. The following section deals with imaging techniques based on light transmission. The last section covers the interaction of human tissue with light.

2.1. Basics of light transmission in optical fibers

The physics of optical fibers rely on relatively simple principles since the general dependencies between parameters (*e.g.* diameter, refractive index) are known. To finally produce a good optical fiber with selected, precise, reproducible characteristics is, however, not a trivial task. The influences of the production of optical fibers on the performance will be discussed in further detail in **Section 3**.

The concept of optical fibers is based on total internal reflection at the interface of core and cladding, their innermost and adjacent layer. This is achieved with a lower refractive index of the cladding compared to the core. While core and cladding are responsible of light guiding, the jacket protects the fiber from external influences and forms the outermost layer. Influences include mechanical impacts, UV light irradiance, heat, and the chemical surrounding. For body-monitoring, light is intended to interact with the surrounding media *e.g.* human tissue during body-monitoring. Therefore, optical fibers without protective jackets are normally used for sensing applications and thus consist of only two layers.

For light propagation through the fiber, the critical angle ψ_c for a total reflection is given by **Equation (1)**:

$$\psi_c = \arcsin\left(\frac{n_{cl}}{n_{co}}\right) \quad (1)$$

where n_{cl} *[-]* is the refractive index of the cladding material and n_{co} stands for the refractive index of the core material. For incoming rays with an angle larger than ψ_c *[°]*, total internal reflection is achieved as marked as the shaded area in **Figure 1**. ψ_c is the minimum angle from perpendicular at which a ray entering the optical fiber will be guided. The values can vary strongly with material and geometry of the fiber. [20]

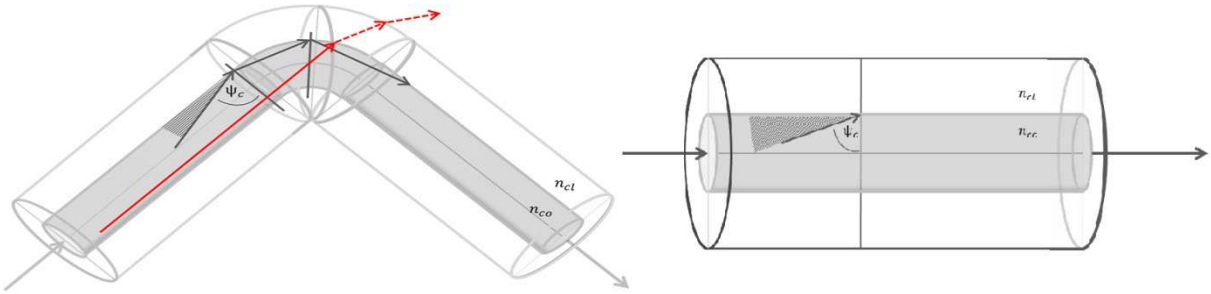

Figure 1: (left) Bent fiber including schematic ray paths: (black) A ray is reflected internally around a bend, (red) A ray reaches the interface at an angle ($\psi<\psi_c$) and is thus transmitted, (right) Condition for total internal reflection: Shaded area gives possible angles ($>\psi_c$) of incident for rays in an optical fiber. n_{co} and n_{cl} denote the refractive indices of core and cladding respectively; radii of core and cladding are not to size.

In fiber design, the radial variation of the refractive index can result in significant changes for transmission of light in the fiber. Generally, one can differentiate between three different designs: Step-index fibers are optical fibers with a constant refractive index across the core. In contrast, graded-index and multistep-index fibers have a varying index. Graded-index (GI) fibers are characterized by an radially continuously decreasing refractive index in the core material. Multistep-index (MI) fibers show stepwise changes in refractive index, for each of which a separate interface exists. Optical fibers are not only characterized by their refractive index profile but also by the number of waveguides traveling through the fiber: to differentiate between single-mode and multi-mode fibers, the normalized frequency V is given by **Equation (2)**) [21]

(2)

$$V = \frac{2\pi a}{\lambda}\sqrt{n_{co}{}^2 - n_{cl}{}^2}$$

where *a [nm]* is the core radius and *λ [nm]* the wavelength traveling along the fiber. For values above 2.405, the behavior of step-index fibers is multi-mode. Below this value, resulting as the first root of the Bessel function, only a single mode is guided in the respective fiber. The number of propagation modes for multi-mode fibers is calculated with

(3)

$$N = \frac{V^2}{2}, \text{if } V \gg 1$$

with *V [-]*, the normalized frequency (as calculated in **Equation (2)**). In this review, the value *N* is considered in respect to the bending light loss of fibers used in various applications. The value itself is discussed in the following in the context of modal dispersion.

Figure 1 intrinsically also shows the higher sensitivity of single-mode fibers to bending: Single-mode fibers show high values of ψ_c, leading to the requirement of considerably straight ray paths along the fiber. In a bend, the light ray meets the interface of core and cladding at a small angle ψ and thus cannot be totally reflected inside the fiber (comparable to the red path given schematically in **Figure 1 (left)**, with angle ψ_c close to 0°).

The usability of an optical fiber can be also characterized by its bandwidth. The bandwidth defines the information-carrying capacity. A single-mode glass fiber allows for transporting of high data rates or, correspondingly, a high bandwidth capacity. The high bandwidth capacity is achieved as one traveling mode excludes the effect of modal dispersion. The effect is defined as the dispersion in arrival time of rays at a given length of an optical fiber. Rays traveling along a multi-mode fiber show modal dispersion due to varying total traveling distances, proportional to each ray's guiding angle. Hence, modal dispersion of fibers restricts the transmission rate. Generally, the dispersion scales with the core diameter. Polymer optical fibers with prevalently large cores thus show a higher modal dispersion. The variation in path lengths is due to the commonly higher number of traveling modes as well as the larger maximum length at the same guiding angle. The transmission rate for POFs can only be maximized by reducing the dispersion. Mode coupling is one way to reduce modal dispersion. The input signals can then be switched between different modes at different times, resulting in an averaged group velocity. The waveguide system has then established an equilibrium mode

distribution. [22] Alternatively, the use of graded-index fibers with higher transmission speeds in their lower-index areas compensate for the longer paths of the faster modes. [23]

Finally, very important optical properties are attenuation values, the extinction losses, and the tenability of the optical fibers. Light intensity decreases with distance *z*, with a given attenuation coefficient α *[dB/km]*. Influences on extrinsic losses are among others: Absorption from pollutants and dispersion at *e.g.* bubbles. [21] Most important though, as the phenomenon is exploited for body-monitoring devices, is the attenuation resulting from micro- and macro-bends. [21] These types of losses are used in many applications for the controlled out-coupling of light. To differentiate, macro-bends induce light loss due to excessive bending of the fiber while micro-bends are caused by deformation of the fiber, *e.g.* during manufacturing or localized pressures. Thus, micro-bends are of a size of the fiber diameter while macro-bends occur already at larger curvature radii. [21] Both of the bend types are utilized in optical fiber sensors. A fiber with a macro-bent loop is shown in **Figure 2**. [24] The fiber was designed to show low bend losses by optimizing the individual bend losses but also the group delay characteristics. High bend tolerance is characterized by optimally constant light attenuation throughout straight and bent sections of a fiber. The high bandwidth is preserved and such a fiber is thus compatible for communication applications.

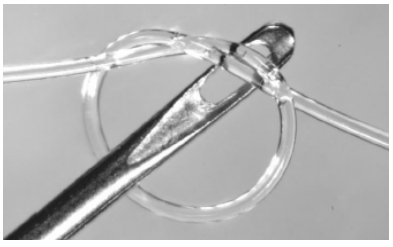

Figure 2: Tight bend of a multimode fiber. This example was designed to show low losses in bending situations primarily used for communication purposes [24], reproduced with permission by © 2012 SPIE.

Exploitation follows careful adjustment of the parameters influencing bend losses. These are cladding thickness, fiber core diameter, bend radius, number of bends and their length and the fiber environment. (Global) numerical aperture, refractive-index profile or in-coupling conditions stay constant with a chosen fiber type. [25] The decrease of power is higher at smaller bend radii and thinner claddings. Sharp bends thus out-couple high amounts of luminous radiance *I*, as they eliminate higher modes traveling close to the critical angle. It has been shown that a bend cannot be treated individually but rather depends on the fiber alignment in proximity: The local distribution of rays within a fiber changes while the light is passing through a bend. [26] Correspondingly, in a ray-tracing model as utilized in multi-mode fibers, the starting positions for the following recursive step after a bend are no longer evenly distributed. Furthermore, the distance between two deviations from a straight fiber (denoted *D* in **Figure 3 (left)**) influences the curvature losses, although the losses are independent on the curvature's direction in consecutive bends. [27] A measure for fiber performance has been proposed as the slope of curvature losses *versus* the number of bends, which correlate to the mode coupling. Coupling strength, in general, can be visualized with the pattern changes of fiber output power in far-field, describing the angular properties of the electric field. [28] For the equilibrium, a ring pattern is seen. The coupling strength is then linearly proportional to the length due to its exponent at unity. [22]

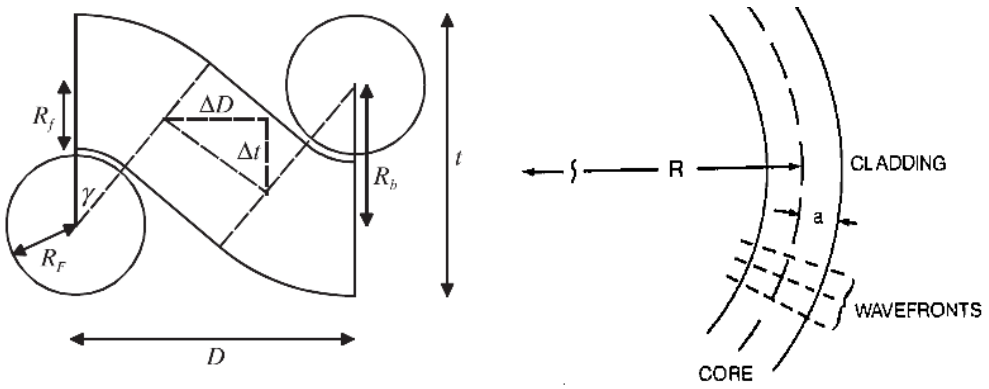

Figure 3: (left) Schematic for the bending of a fiber integrated into a woven reinforcement fabric, including denominations for calculation of bend [26] reproduced with permission by © 2008 IOP

Publishing Ltd, (right) Curved fiber with progressing wave fronts: The velocity of the wave fronts varies in the optical fiber in a bend as seen with a longer distance/time unit at the outer surface of the fiber [29], reproduced with permission by © 1991 Optical Society of America.

Great interest lies in finding a reliable computation method for fiber losses for body-monitoring applications. Whichever optical fiber is used and for whatever application, a luminance output is the basic material value to be known. Many different computation methods have been proposed. A very extensive mathematical derivation was published by Smink, de Hon, and Tijhuis (2007). [30] Straight-forward approaches evaluate the losses in power by looking at the contained power per unit area of a sufficiently long straight fiber section. For this, it is usually assumed that all rays entering the bend have identical power, corresponding to the optical power density per unit cross-sectional area. Hence, the change of power per area depends on the maximum luminance, the angles at which the rays are traveling and the solid angle. Considering only rays without radiation loss in the core, **Equation (1)** can be modified into **Equation (4)**

(4)

$$\partial P/\partial A = K * (n^2 - n_{cl}^2)$$

with *K* as a constant. The luminance is thus isotropic. [31]

For a bent fiber, the velocity of propagation of a wave front increases with the distance from the center of curvature (**Figure 3 (right)**) until it equals the local velocity of light. At higher velocities, the ray cannot be guided anymore and is radiated off. Power loss attenuation can then be related to the fiber properties (*e.g.* core radius) and bend geometry (*e.g.* bend curvature). [29] With the general equation for power in a guided mode after propagating a distance *l* (given in **Equation (2)**), and the knowledge that a large number of modes *N* (given in **Equation (3)**) exist, the total power can be assessed integratively. Finally, the proportion of lost optical power is calculated as the ratio of the power remaining in the fiber in comparison to input power.

To use optical fibers for the measurement of vital parameters, they have to be connected to a light source and detector. Regarding the number of fibers, several configurations are possible: A single fiber for excitation and collection, a single fiber for excitation and multiple fibers for collection and finally fiber bundles for excitation and collection. [32] Each of these configurations show advantages and drawbacks, *e.g.* while a single fiber only detects emission from a small surface, its connection system is simple. A fiber bundle demands a much more complicated connection system but receives light from a larger surface. Furthermore, changes in light output have to be ascribable to a specified area on the fiber while light in-coupling efficiency to the fibers varies significantly. Thus, the light-incoupling technique (into the core or from the side) leads to varying photosensitivity effects and phase shifts. [33]

A very important sensing principle is realized with Fiber Bragg gratings (FBG). They were developed to receive tailored responses independent of the absolute input value. The FBG

sensors only require one strand and relatively simple imaging techniques. [10a] They generate wavelength shifts that can be designed and manufactured uniquely for each grating position. For the measurement of several parameters at once, FBGs can be used, e.g. by superimposing gratings at the same position of the fiber. [34] Simultaneous measurement at several positions of the fiber is achieved by different grating distances. The gratings can be introduced into the fiber in different ways: By a phase mask, direct writing, or a combination of phase mask and interferometry. [34] During use, the pattern back-reflects wavelengths specified by the grating. Constructive interference of the scattered light is only observed for the Bragg wavelengths which are given by **Equation (5)**.

(5)

$$\lambda_B = 2n_{co} * \Lambda$$

where n_{co} *[-]* is the effective refractive index in the core and Λ *[nm]* the period of refractive index modulation. The Bragg wavelength relates the periodicity of the grating to the effective refractive index of the core. Perturbations in either of these parameters, which are dependent on strain and temperature, result in a wavelength shift. FBG sensors allow real-time sensing of strain, temperature and vibration. As the shift in wavelength is measured, the absolute value is independent of fluctuations in the irradiance source. [34] However, with careful selection of the parameters, the reflected power in dependence to the temperature and other external effects can be maximized. Unwanted effects are micro-bending leading to decreased intensity of reflected signal as well as chirping (a variation in either grating period or refractive index) resulting in a distortion in Bragg wavelength. [35] Additionally, a narrow peak is only possible for single-mode fibers. These then allow for a simple relation between wavelength shift and periodicity of grating.

(6)

$$\Delta\lambda_B = \lambda_B * n_{eff}(\alpha, \xi, p) * \Delta X$$

As given in **Equation (6)**, sensing is based on the external parameter *X* (*e.g.* temperature or strain). The parameter induces a change in effective refractive index which then in turn alters the Bragg wavelength. The effective refractive index n_{eff} depends on various material coefficients related to the external influences *X* . The effect of such grating is seen in both the transmitted and reflected spectrum both of which can be used for detection. While a FBG already provides a wavelength-encoded technique, chirped gratings even offer dispersion compensation or serve as a wavelength bandpass. [34] The latter is constructed to back-reflect many wavelengths. Exemplary methods to achieve chirping are tapering of the FBG or an introduced strain gradient along the grating. [36] To ensure a longer life-time, FBGs are burnt-in as well as strained above measurement range before use. With these measures, the gratings are annealed and relaxation effects are eliminated. [37] The annealed POFs then show a higher thermal threshold and an enhanced elastic limit as well as a lower attenuation in strain. [38] For an ideal measurement, no hysteresis or drift should be seen. Furthermore, the parameters are supposed to be single-valued. These prerequisites are verified when a grating is produced. Regarding a specific response for a desired parameter, the loading and unloading has to be reproducible and reversible. During the unloading process, the strain on the fiber is released and the response should – in an ideal case – return to the zero stress state. The deviation from the purely elastic response defines the extent of lost energy due to viscoelasticity of the polymeric material. Usually these two evaluations limit the maximum tunable Bragg wavelength shift, *e.g.* 32 nm for a polymethyl methacrylate (PMMA) based POF grating. [39] To customize the properties for a specific application, different approaches are used. Their thermo-optic and electro-optic properties as well as the strain sensitivity with fiber Bragg gratings is very high. Inversely, a specified wavelength response can be achieved by varying the tensile stress or the temperature. The sensitivity for a wavelength change is reportedly

higher for POF gratings. [39a, 40] A very useful property of Bragg grating optical fibers is their multiplexing capability. [41] This advantage can be seen in **Figure 4**: Bragg gratings with different grating periods along one fiber show specific reflected and transmitted spectra. The reflected wavelengths correspond to the back-reflected wavelengths of the gratings and the missing wavelengths are visible in the transmission spectrum as well. [42] Finally, FBGs can be considered to have a small sensor footprint, being non-invasive with a very low mass and heat capacity, hence virtually not changing the system. [37] The advantages are manifold: The measurement resolution can be improved with sharp peaks, and a multiplexed use of the sensor is possible. [43] A relatively new development was a single frequency laser achieved with a polymer optical fiber Bragg grating: The grating was used as the reflection mirror for creating a laser beam. [43] Under applied strain to the fiber, a grating distance modulation was achieved. This modulation then changed the Bragg wavelength.

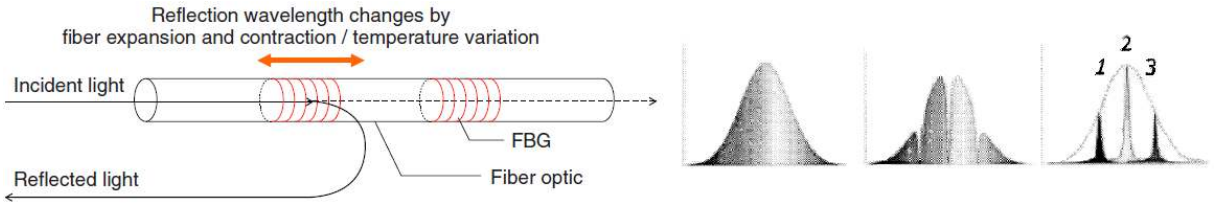

Figure 4: (left) Schematic of a FBG sensor [44], reprinted with permission from © 2013 ElSevier, (right) Input spectrum, transmitted spectrum and reflected spectrum for 3 FBG sensors with different grating distances along one fiber [42], reproduced with permission by © 2005 SPIE.

Finally, multi-structured polymer optical fibers can be grated to provide both the advantages of Bragg grating as well as the higher photosensitivity with doped cores. Many possibilities arise for adjusting distribution of dopants, the microstructure, and the grating. [45] Liquid-core optical fibers show very high sensitivity, especially through their Rayleigh scattering response and have been used to measure refractive index changes. [46] If a medical condition results in a refractive index change, these fibers could be beneficial to use. Liquid-core optical fibers are reviewed in more detail elsewhere. [47]

2.2. Imaging techniques based on light transmission

The commonly used imaging techniques based on LEDs and photodiodes can also be applied with optical fibers. **Section 2.2** thus serves as a connection between the basics of optical fibers and the interaction of light with tissue, including scattering effects and the resulting light ray paths through inhomogeneous matter.

Contrary to fiber Bragg gratings which were treated as optical phenomena, the following techniques use unprocessed optical fibers. Hence, structural changes are neither made in the cladding nor the core of the fiber. **Near-infrared spectroscopy (NIRS)** is one of the most common techniques using at least two wavelengths to illuminate the tissue. It is an optical non-invasive tool using monochromatic light sources or filtered white light with wavelengths of 650-1000 nm. The strongest absorbers in that region are intravascular hemoglobin (both oxygenized and deoxygenized), oxygenated and deoxygenated myoglobin, and cellular cytochrome oxidase. [48] From the oxygenation information, a function can then be derived to determine indicators *e.g.* on muscle metabolism. [49]

Laser Doppler flowmetry (LDF) is based on frequency shifts between incoming and reflected light. Doppler-broadening is seen as a result of light being reflected at a moving scatterer. The light source is a continuous laser. The Doppler shift is normalized at the desired light intensity logging the intensity fluctuations. The signal gives a value for perfusion (red blood cells in movement) in the venous system independent of the skin composition. [50] Furthermore, the tissue blood flow in various tissue types and organs can be evaluated.

Tissue viability imaging (TVI) uses linearly polarized white light. Thus, with the use of visible wavelengths, the method becomes sensitive to melanin. As a result, the data represents the difference in absorption between erythrocytes and the surrounding tissue. However, while the skin-type has no effect on the accuracy of LDF and NIRS measurements, TVI shows a

change between subjects with darker and lighter skin types. [50] The reason is that melanin absorbs green light more strongly than red light (comparably to red blood cells) and thus let darker skin appear to have a higher erythrocyte concentration.

To filter the reflected light from the skin surface, a crossed polarizer is used. Therefore, the only light that can pass is scattered light. Hence, only the microcirculation in deeper dermal layers is monitored. These measurements can give information on the skin blood volume of the patients.

Pulse oximetry uses molecule-specific wavelength absorbance by illuminating the tissue at several wavelengths, usually two. The tissue is usually examined in transmission thus only on thin body parts. Pulse oximetry monitors the oxygen saturation in the blood through flashed pulses of red and near-infrared light. [51] The intensities of the transmitted light changes with the arterial filling corresponding to the heart beat. The light attenuations for the absorbance of both red and infrared light are high-pass filtered to remove the baseline, the remainder being the amplitude of the acquired data which reflects the spectrum of the arterial blood. [52] The absorption of the different hemoglobin constituents is prominent in this range and red and near-infrared light is thus ideally suited for non-invasive blood analysis.

Photoplethysmography (PPG) is used to assess blood circulation and – importantly – also its diminishment. For a PPG measurement, LEDs or laser can be used as a light source. Often a pulse oximeter is used for illuminating the skin and the change in intensity is used for the volumetric evaluation of the contained arteries. The two chosen wavelengths lie within the red and near-infrared spectrum of light. [53] Set-ups with a combination of green and NIR light are also known. [54] Green light is more strongly absorbed by blood than NIR light and the green light source is therefore adjusted closer to the detector to receive signals. The AC component of the signal is attributed to pulsatile changes in blood volume and blood flow (including pressure variations and orientation of the red blood cells) corresponding to the cardiac cycle with systole and diastole. [55] The DC component shows changes in the total blood volume.

Intensity variations can be ascribed to vasomotion, thermoregulation and respiration. [56] Controversially, Binzoni, Tchernin, Hyacinthe, Van De Ville, and Richiardi (2013) have stated that the intensity fluctuations are not related to the blood flow but to a variation in reduced scattering and absorption coefficient. This variation is ascribed to the red blood cell deformation and orientation to the PPG probe. [57]

Pulsations vary with proximal or distal attachment of the sensor as well as with the left and right side of the body. Differences between the sides of the body at the same position are naturally small, as can be seen in **Figure 5 (left)**. However, for patients with a vascular disease or autonomic dysfunctions, the right-to-left side similarity is drastically decreased. In **Figure 5 (right)** an example is given for an artherosclerosis occurrence in the distal extremity, seen from the toe PPG signal. The PPG signal also gives information on endothelial function, venous insufficiency, anaemic conditions, neurological variations and microcirculatory dysfunctions among others. [58] A reference PPG signal then shows the patient-specific changes from a baseline condition. [58] Quite recently, PPG measurements were also introduced for the observation of bone hemodynamics during occlusion of blood flow. [59] To conclude, PPG is a versatile tool to assess human variance and even detect risk factors or diseases even though not all wave-form characteristics are understood.

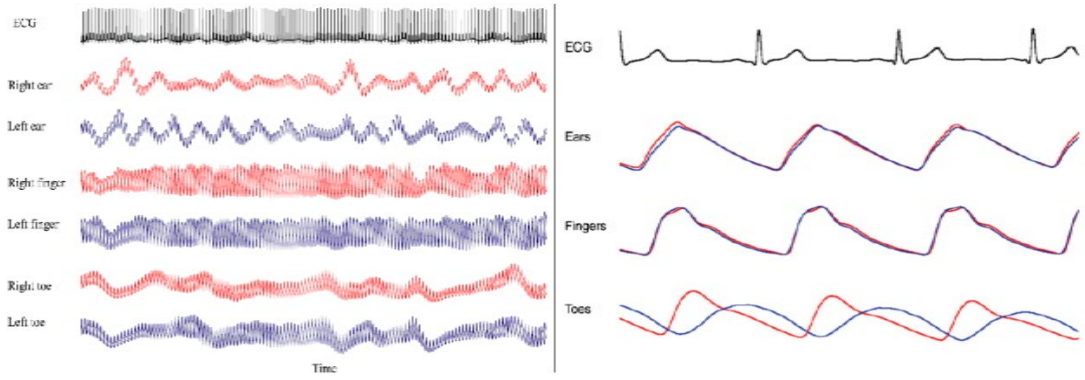

Figure 5: (left) Comparison of output signal for ECG and PPG graphs. For the latter, the signal for both left and right side for ear lobes, index fingers, and great toes is logged and similarities can be seen between the body sides, (right) PPG recording for multiple locations both left and right. A unilateral lower limb atherosclerosis can be seen from the damping and reduction of amplitude of the affected side as well as the

relative delay between the both toe-signals. The similarity between the other pulses shows no other considerable proximal arterial disease [58], reproduced with permission by © 2007 IOP Publishing Ltd.

Overall, the discussed non-invasive optical techniques all take advantage of the different absorption spectra of specific constituents at different wavelengths. For TVI, polarization filters help restricting the detection of scattered light, excluding reflected light. LDF then uses a frequency shift due to reflection at red blood cells, while NIRS and PPG log the absorption at hemoglobin variants and erythrocytes respectively.

2.3. Optical properties of skin and biocompatibility of sensors

How light penetrates the tissue is an important factor for biophotonic healthcare monitoring applications. At the surface of the skin, the incident ray may be reflected. In the tissue, scattering and absorption are predominant (**Figure 6 (upper right)**). Blood is the main absorber in the tissue within the visible and NIR spectrum. The depth of light traveling through the tissue depends on absorption and scattering coefficient. [60] The latter being strongly related to the structure of the tissue. [48, 61] While human tissue is anisotropic and inhomogeneous, these properties change not only with the age but also with the pathological condition. [62] Depending on the wavelength, oxygenated and deoxygenated hemoglobin absorbs differently. Reversely, for known reference values, changes within the tissue, *e.g.* malignant tissue, can be identified with the scattering properties or the hemoglobin concentration. [63] These measurements rely on knowing the depth that is reached in the tissue, approximated with the decreasing optical radiation. Such, the depth is often taken at which the radiation density has decreased to *1/e* of the initial value. [61a] Tissue as a multiple scatterer of light generally varies greatly in optical properties. [64] Hence, to understand the interaction, not only practical studies were conducted but also many modeling approaches were used. Soft tissue scattering, for example, was looked at with a discrete particle model. [65]

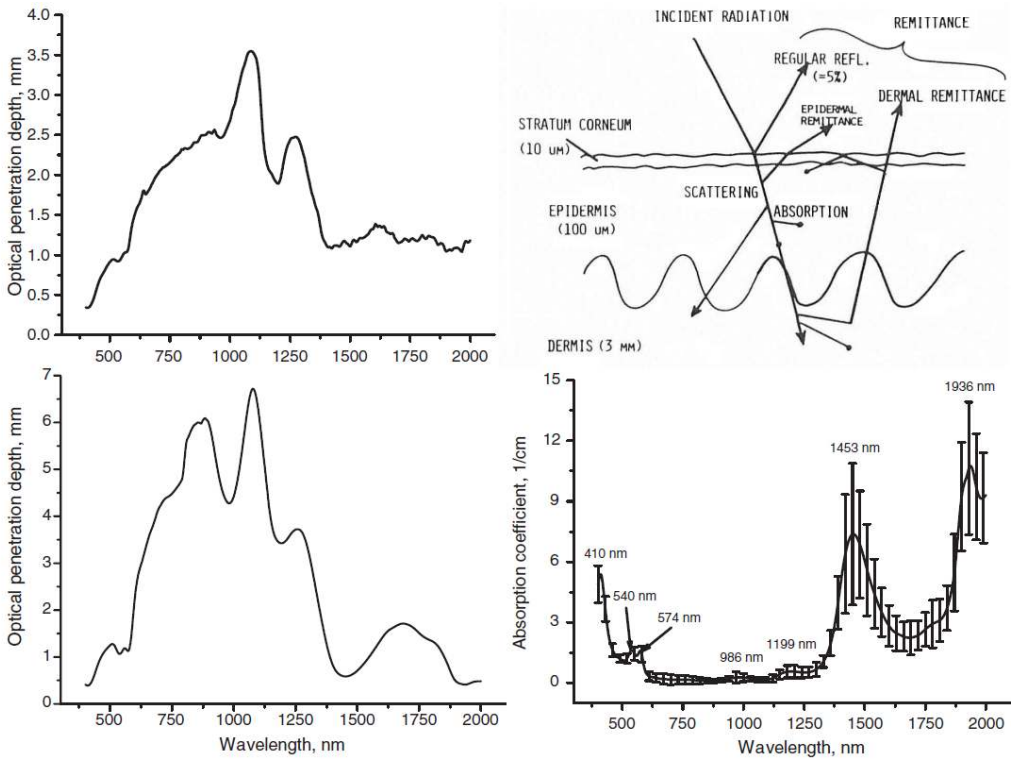

Figure 6: For post mortem examinations: (upper left) Optical penetration depth δ of light into human skin, (lower left) Optical penetration depth δ of light into human mucous tissue over the wavelength range from 400 to 2000 nm which shows a clear difference to the graph for skin above [66], reproduced with permission by © 2005 IOP Publishing Ltd (upper right) Schematic diagram of optical pathways in skin [61a], reproduced with permission by © 1981 The Williams & Wilkins Co, (lower right) Corresponding to the optical penetration depth into mucous tissue, the absorption coefficients μ_s is calculated with IAD (inverse adding-doubling) method in dependence of the wavelength; (solid) Averaged experimental data, (vertical) Standard deviation values [66] , reproduced with permission by © 2005 IOP Publishing Ltd.

From the different modeling results, it has been concluded that the reduced scattering coefficient is dependent on Mie and Rayleigh scattering, with Rayleigh scattering dominating in the visible wavelength. [66] It is dependent on the used wavelength. For mucous tissue, the variation of the absorption coefficient with the wavelength can be seen in **Figure 6 (lower left)**. Furthermore, a significant change in penetration depth is observed in different tissue types, *e.g.* for skin and mucous tissue (**Figure 6 (left)**). [66] Mucous tissue shows different local maxima for the optical penetration depth than skin. It has been shown that larger

distances between light source and detector provide more optical information about deep tissue. [67] It has to be taken into account though that absorption and scattering events are temperature-dependent as well as that deflection varies in magnitude with the measurement subjects. [68]

The term biocompatibility includes the toxicity of the material, its inertness, and finally comfort. Regarding the subjective comfort, friction between sensor and skin is a very important parameter. For this, the friction of the substrate material is determined including the optical fibers. Additionally, the *stratum corneum* water content can be measured leading to dry skin which influences the friction of material on skin. [69] Skin irritations can lead to painful infections and have to be prevented. [69] Variations of the skin climate have to be taken into account, such as that even subjects with *xerosis* or *atopic dermatitis* are targeted for the sensor usage. Not only is comfort influenced by mechanical but also by chemical properties. [69] Discomfort is caused by moisture in the clothing as well as coldness to touch of the fabric. Additionally, the perception of dampness is influenced by the hygroscopicity of the material. [70] Finally, safety regulations regarding toxicity of the garments have to be complied with. Not only are the light guiding properties of the tissue important but also its interaction with optical fibers. Allergic reactions or mechanical interactions with the optical fiber have to be prevented and therefore the materials for all medical applications have to be selected carefully. Many optical fibers have shown good biocompatibility, being used in in vitro invasive measurements to determine strain in bones and in tendons. [71] Optical fibers from *e.g.* silica are generally biocompatible. [10a]

3. Materials for optical fibers

By now, many different materials have been tested and used for the production of optical fibers. The most commonly known materials are silica (among glass optical fibers) and PMMA with a fluorinated coating (among polymer optical fibers) due to their wide application in the communication sector, both being lightweight and compact. [16b] Generally, besides the processability, only the prerequisites of optical transparency and flexibility restrict the material selection. Optical transparency is usually achieved for amorphous materials, if the polymer contains no absorbing group. Amorphous materials consist of statistically oriented molecules. For glasses, the condition is accomplished due to fast quenching. There, not only silica, fluoride glasses and chalcogenides have been tested but also crystalline materials, as well as various copolymers and dopants. These can also be used for refractive index modulation, depending on the specific processing parameters of the materials. [15, 72] For polymer optical fibers, many materials are available: polystyrene, polycarbonate, polyolefins, and perfluorinated polymers among others. [73] Doping is feasible as fine-tuning of the refractive index in most POF productions due to the comparably low processing temperatures in the drawing process. [74]

Manufacturing methods include extrusion, thermal bulk polymerization, photo-polymerization, chemical vapor processes, fiber drawing (thermal scaling of a preform), and interfacial gel-polymerization. [16b, 18, 73, 75] The methods all have different advantages and drawbacks such as conversion of the monomers or time consumption. The choice of the processing method is influenced by the amount of contamination or limitations in controllability of *e.g.* the layer thicknesses or uniformity. Therefore, silica is preferably purified using chemical vapor deposition techniques. High purity can be achieved due to the large difference in vapor pressure of tetrachlorosilane (reacting halide) compared to possible impurities. [72d] For all methods, gas bubble inclusion has to be prevented, *e.g.* with pressure or degassing of the material before and during processing. In blends, the macro- and microrheology of both

components is important. [72c] Depending on the process, the production can be established continuously at high speed. Exemplarily, co-extrusion processes allow high output production. [75]

As with most materials' properties, the optical and mechanical performance of the fibers is dependent on their chemical composition. Blends of polymers as well as additives to a polymer type can improve mechano-physical properties and diversify the structure, the geometry, and the thermal stability. Naturally, the optical properties can also be optimized, *e.g.* by the addition of polymer particles before synthesis. [76] The hydrophobic behavior may be changed as well as the electrostatic behavior. In production, the processability is important and constantly improved upon. Therefore, when working with composites, the miscibility of two or more components has to be ensured at the wished concentrations. [72c] However, exact values (also for thermal and mechanical properties) are impossible to predict as material grade, production technique, post-processing, and complementary armamentarium in measurements all influence the physical property values of the end product. The performance can vary by several orders of magnitude by changing one process parameter. Regarding the light guiding phenomena, different fiber materials show different sensitivity to the phenomena described in **Section 2**. However, this response again varies with external influences such as a change of the humidity or temperature possibly leading to hysteresis or nonlinear responses. [19, 77] It has been noted in the feature article by Ballato and Dragic (2013) that the paradigm of designing properties via structure and processing holds true for *e.g.* photonic crystal fibers. [72d] Finally, interconnectivity of several processing parameters can bring additional benefits, as shown by fiber-drawing during post-processing for the improvement of resilience. In this example, the drawing temperature is decisive. While lowering the temperature normally enhances the drawing efficiency, a temperature below an optimum value decreases the transparency of the fiber. Another example illuminates how material imperfections influence the performance of fibers in different aspects at once: Polymer optical fibers with impurities in the material show

a lower glass transition temperature nevertheless showed high mode coupling as a consequence of random perturbations. [22] Hence, deciding on a material for optical fibers, one can choose from many options to find the most appropriate for the desired application. The following section is thus meant to introduce a few material examples for interesting features. For textile integration, PMMA, PC, and PS are rather stiff in comparison to conventional textile fibers and yarns though show a significantly lower tensile modulus than silica. [78] These materials, however, do not produce shards when breaking. Tuning the flexibility can then be achieved by *e.g.* an increase in viscosity with increasing molecular mass. For instance, PMMA shows brittle behavior below a molecular mass of 10^4 Da while it is ductile above 10^5 Da. [74] Not only does the mechanical behavior change with the molar mass, but also the refractive index. [79] When a very low attenuation is desired, silica fibers are still the best solution, however showing a much lower flexibility than polymer optical fibers. Concerning thermal stability, the commonly-used PMMA for the POF production has a far lower softening onset than silica. Research on higher thermal stability can still lead to much-improved fibers. The molecular structure of thermally more stable polymers can be investigated; copolymers can be introduced as well as cross-linked polymers or additives. When optical fibers are used in conditions of high humidity, fluorinated polymers are commonly used to prevent moisture penetration into the polymer fiber. [21]

Exemplarily, the thermoplastic silicone elastomer Geniomer (Wacker Chemie AG) is a copolymer combining the properties of two polymers. The advantageous properties of both materials are tuned to receive an improved end product. The silicone part contributes to the suitable optical transparency and very good flexibility as well as to the elastomeric properties. The polyurethane makes up the hard segments of the copolymer and is responsible for the thermoplastic characteristics. [72b] Using this combination, a fully elastic deformation is obtained which can facilitate the production of touch transducers as well as sophisticated load

monitors. [72b] By varying the copolymer ratio, the sensitivity towards applied forces can be tuned, since the varying yield strength dictates the light transmission response. Furthermore, axial strain and bending lead to a decrease of light transmission.

A further influence in performance of fibers is the intrinsic absorption which is dependent on the wavelength. The absorption spectra of the materials depend in large parts on the respective eigenfrequencies. Active oscillations of molecular groups can thus be seen due to their influence on absorption. The absorption curve is determined by the relation of $n^2\kappa$ to the wavelength. The refractive index n and the absorption index κ can in turn also be related to the absorption coefficient a. Due to the often-used multicomponent systems, only the local group oscillations are strongly detected, such as C=O double bonds or C-H stretching vibrations. [80] The different oscillation causes for the C-H group are shown in **Figure 7**. Depending on the wavelength, a different oscillation cause prevails in increased attenuation.

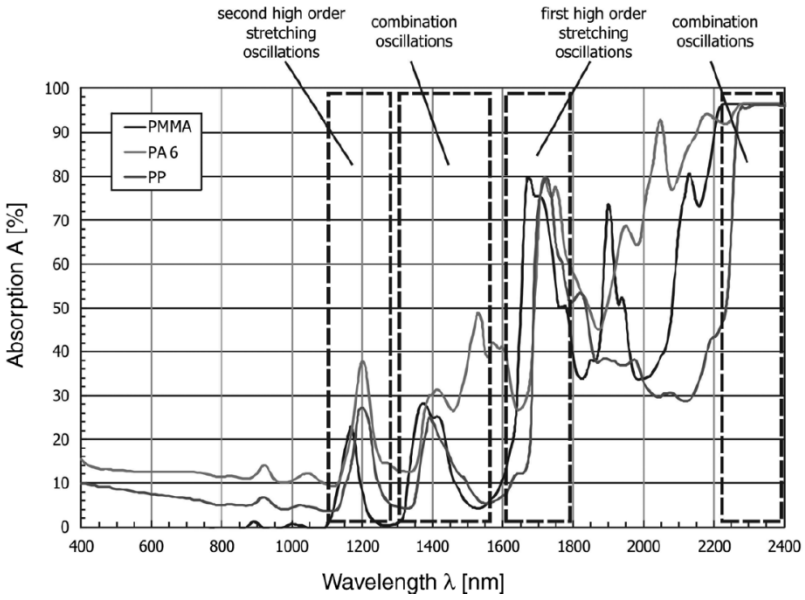

Figure 7: Oscillation-induced changes in absorption for natural PMMA, PA6 (poly(amide-6) and PP due to molecule-specific C-H groups. [81], reproduced with permission by © 2011 Wiley-VCH Verlag GmbH & Co. KGaA.

Property-wise, silica shows the lowest attenuation (at a specific wavelength) for all wavelengths. In this case, the lowest attenuation lies within the NIR range. The light attenuation of polymeric materials can lie between decibels per kilometer up to a decibel per meter range. However, lower attenuations can be realized for specific wavelength regions. The perfluorinated polymer CYTOP®, for instance, is highly transparent in the red region of the visible light spectrum. [16b] Therefore, materials that are optimized for the telecom window of ~1.2-1.7 µm are not necessarily feasible in the applications using visible light. Hence, while choosing the material for an application, the wavelengths that are used have to be considered.

Considering the textile integration, some polymeric materials are being developed to show considerable strength (similar to conventional yarn) with a high tensile modulus while still being highly flexible. These attributes can be shown in dynamic mechanical analysis (DMA) giving information on the viscous and elastic portion of a material. With this method, it was demonstrated that yarns can have a wide spread of property values. [78b] The polymeric fibers can then be varied and interchanged to create a property spectrum as similar as possible comparing to yarns. With these, homogeneous textiles with integrated sensors are feasible.
In the temperature range which is unproblematic for humans, all common fiber types can be used. While polymers melt or decompose at significantly lower temperatures than other material classes, their usage temperature usually exceeds the application range in which humans exist. The sensors can thus be worn in all climatic situations. Contrary, the resistance to solvents has to be evaluated on a case-to-case basis depending on the exact chemical composition of the fiber.

4. Applications

Glass and polymer optical fibers have been used to measure the skin temperature, the respiratory rate, the lung volume, the pulse and the heartbeat, as well as the blood pressure. [82] Furthermore, oxygen saturation and hemoglobin concentrations were logged. [51, 61b, 83] Perfusion in respect to the velocity and concentration of erythrocytes was mainly studied in the field of decubitus prevention. [54a, 55] Regarding the monitoring of movement and stress on the body, pressure and shear stress mapping of body tissue, as well as mobility, actimetry, and gait supervision are possible. [72b, 84] Finally, analysis of target molecules using optical fiber means is used to implement wound monitoring or the measurement of sweat, humidity and pH value. [73, 84c, 85]

This section presents various reported applications of optical fibers for body-monitoring or sensing. While basic parameters can also be measured easily with conventional electrical components, fiber optic set-ups allow simultaneous measurement of several parameters as described in **Section 4.9**. Again, only a selection of examples is given in this section, since many approaches exist. Deviating from polymer fibers, planar waveguides are considered for **Section 4.10** as they can be strongly tailored due to their single mode nature. Examples in an advanced stage of development were focused on.

4.1. Respiration – Supervision and Aid

Respiration supervision is a very important task in patient healthcare *e.g.* in critical care units. Breathing is controlled by the medulla oblongata together with other autonomic functions. [86] This part of the brainstem sends information on the oxygen concentration and carbon dioxide exchange but also on the volume of inhaled air (discussed in the following **Section 4.2**). Furthermore, by measuring the frequency of breathing, the psychophysiological state can be influenced. [87] For instance, slow and deep breathing as well as longer duration of exhalation than inhalation can reduce the skin conductivity levels. While intubated, respiration still needs

to be detected to synchronize the – though possibly feeble – patient respiration rate and the support by the machine. Thus, the natural rhythm is strengthened and not impaired by a machine-dictated rhythm. In comparison, the positive pressure ventilators create an increase in pulmonary vascular resistance and a decrease in cardiac output. [82b] Respiratory failure can also be caused by cross-talk between various organs. [88] Acute kidney injuries can for instance prompt an enhanced inflammatory response causing a uremic lung. These cross-talks in pathophysiological conditions are highly dangerous, still causing a high mortality rate. [88]

A specific application is the monitoring of respiration for patients suffering from sleep apnoe syndrome at night. The syndrome manifests itself with reduced and irregular breathing. Since sleep is very important for the daily recovery of energy, the patient's health status can be derived. Even without a diagnosis why the breathing pattern is abnormal, the entire sleep cycle is informative regarding the patient's health. [89] Therefore, bed sensors for long-term monitoring of breathing help analyzing the condition. For these sensors, the sensitivity has to be high to distinguish between rollover effects and relatively small-scale breathing patterns. A bed including an array of sensors showed the breathing response for various sleeping positions. The signal quality can be improved with optimization of the array position and filtering of artifacts resulting from *e.g.* rollover movements. [89]

Two different optical fiber -based monitoring techniques were used for breathing monitoring: PPG (see **Section 2.2**) and optical strain-based sensors. [82g]. The breathing patterns can easily be read from the PPG signal. [90] In strain-based sensors, modulation of light intensity can be ascribed to the extend of elongating the optical fiber. Another proposal for the strain sensor is micro-structuring (heterocore and micro-structured fibers) as heterocore fibers have shown high sensitivity to macro-bending. [89] These fibers are highly sensitive to bending but independent of temperature changes. As an advantage over general polymer optical fibers, these sensors were built with single-mode transmission fibers,which are less susceptible to external influences. [89] Therefore, they can also be used for precise pressure sensing

applications such as post-op respiration detection. These RIIVs (Respiratory-Induced Intensity Variations) arise from alterations of the intra-thoracic pressure and the sympathetic tone control of cutaneous blood vessels. It is believed that the autonomous nervous system is involved in the specific components of the PPG waveform as the RIIV still occur in completely occluded body parts. [58]

Besides the PPG sensors, strain-based and macro-bending sensors, FBG sensors, and optical time domain reflectometry (OTDR) sensors have been used. [82f] For flexible and elastic fibers an integration is straight-forward. The maximum elongation of the fiber is correlating to the total body circumference change during deep breathing. [82f] However, the bend loss is not only dependent on the elongation of the fiber but also the used wavelength. [91] Therefore, calibration has to be careful. Additional obstructions are muscle movements. During respiratory supervision, the usage of the muscles around the rib cage leads to deflections. For FBG-based sensors, straight-forward output for expansion under strain is possible by tuning the Bragg wavelength such that the filter spectrum lies on the shorter wavelength side. In that way, the light intensity increases with the extension of the FBG. For a neutral circumference, no response is seen which facilitates the reading of the measured data. [82b]

Finally, another very sturdy sensor has been fabricated with the inclusion of an FBG sensor into a 5-ply laminate from carbon fiber sheets. [82a] This sensor system was produced with a phase mask exposure technique for the FBG writing and unidirectional layers of carbon fiber reinforced plastic (CFRP) sheets. They were placed underneath the mattress and thus effectively eliminated possible pressure spot occurrence. The respiratory rate was in accordance to manual counting. [82a]

A specific example of respiratory monitoring with optical fibers was studied during the European project OFSETH: The sensing of vital parameters was conceptualized in 2006. Part of the project was the development of a harness to measure the thoracic and abdominal breathing movements. Due to the easy introduction of the fiber, several configurations were

compared, namely a macro-bending sensor, an FBG-based sensor, and an OTDR-based sensor. [82f, 82g] For single-mode optical fibers, however, mode coupling occurred and the signal was thus hard to interpret. Additionally, a large drift in the response signal was observed. The FBG-based sensor required certain robustness in the embedding, but it related stresses (elongation of the sensor) linearly to a wavelength shift. [82f, 82g] OTDR allowed the measurement in relation to time and intensity. For that, illuminating pulses were used such that the strain is measured at several locations along one fiber. The backscattered signal was interpreted by photon counting which had to be optimized for the used optical fiber. [82f, 82g] The OTDR signal showed a good correlation to the breathing volume as well as to the respiratory cycles.

Overall, respiration monitoring can be achieved with fiber-optic sensors. Mattrass-based set-ups reliably show the breathing pattern even when the patient is moving. Therefore, the sensors can be used in a home environment reducing the white coat effect.

4.2. Respiration – Lung volume assessment

Lung volume measurements are necessary to receive an input on the gas exchange and supply to tissues. For a known lung volume, the inhaled oxygen can be estimated from the air composition. From this value, the oxygen supply to tissues and organs can be estimated at a given heart rate. Lung volume measurements are linked to the respiratory rate but also to the fitness level of the individual: Activity programs improve lung function and eventually lead to a considerably larger lung volume. [92] Constant shallow breathing can lead to a lower lung capacity. Conscious breathing improves the muscle strength in the chest including general posture. For some respiratory illnesses such as Asthma or *cystic fibrosis*, breathing exercises are essential. For sufferers from these diseases, monitoring of breathing depth and rate can offer relief on a long-term basis. [93]

Even though much research has been done in the field of lung volume assessment, the evaluation is not easy. The lung consisting of extremely fine branches makes an exact value impossible. Usually, an approximation is performed via masks at which the air intake is measured for a complete exhalation and following full inhalation. For these measurements, the total lung capacity (which lies at around 6000 cm^3) still cannot be obtained as the lung cannot deflate completely leaving a residual volume of approximately 1200 cm^3. [94] Furthermore, maximum inhalation depends on the perception of the patient. However, the obtained vital capacity for the individual may give information on air exchange. For these evaluations, one has to keep in mind that overestimations are extremely dangerous at critically low volumes. A relatively simple approach approximates the lung as a conical model evaluating volume change through the variation of rib cage circumference during breathing. [86, 95] Combining measurements of the volume at rest and its change, the lung volume can be determined. With this method, a sensor belt can be used for measuring the circumference change as discussed in **Section 4.1**. [82f, 82g, 95] Elongation relating strain to the changing grating period of the fiber can also be measured. [39b] The strain can then be expressed similarly to a temperature change (**Equation (7)**), derived from the general equation for fiber Bragg gratings.

$$\Delta\lambda_{Bsi} = \lambda_{Bsi}(1 + p_{eff})\varepsilon_z \quad (7)$$

The indicator *i* indicates the *i*th reflection mode, while p_{eff} is the effective strain-optic constant. While elastomeric materials show linear behavior relating strain and stress, viscoelastic materials require polynomial fitting. The resulting values for the material coefficients thus change under applied stress which necessitates larger calibration efforts. [39b] However, the coefficients are not user-dependent.

4.3. Cardiac output – Measurement of heartbeat and rate

The strength of the heartbeat and its rate are very important for a first assessment of health. The pumping of the blood through the heart ensures life. When checked by medical staff, the pulsation can normally be found with low contact pressure on the patient's skin close to an artery at the skin surface. The heart rate gives information on heart irregularities as well as physiological and mental state. Exertion or stress levels can be evaluated. As for cardiac output, a normal stroke volume allows 5 L of blood to pass the heart per minute. [58] With impaired function, as with cardiovascular diseases, the volume can be significantly reduced.

A clinical trial is currently in progress to measure the heart rate, breathing and arterial blood oxygenation with LEDs in reflection mode. [12b, 82c] With these parameters of heart beat and rate monitored with PPG, the researchers want to find criteria that lead to sleep apnoe. [82c] In-ear devices advantageously still receive signals during blood centralization thus being a popular site also for electronic-based sensors. [96] The project has also worked on the reduction of movement artifacts with such sensors. [12b]

For heart rate measurements, optical fibers show an interesting and useful side effect. Compared to an electrical signal, the fiber optic signal is delayed, nevertheless showing both R and T curves as in an ECG. [82h] From the delay in signal, blood flow velocity could be estimated. Schäfer and Vagedes (2013) stated though that PPG-logged rates are not derived from the heart rate but rather pulse rate. [97] The variability between the methods was underlined by an extensive list of studies done on the same topic. Some pathological conditions produce a considerable discrepancy between responses, *e.g.* during physical stress. As the foot and wrist measurements show different delay times, it has been proposed to determine the blood flow velocity as a function of the height of the individual. [82h] Additionally, the obtained signal amplitude and peak sequence depends on the heart's orientation respective to the measurement sensors.

Obtaining cardiac output by optical means is more difficult than the heartbeat. It can be estimated from a PPG by a pulse-contour analysis in which the stroke volume is multiplied by

the heart rate. [58] The estimation proves to be difficult non-invasively. However, with mimicking the aortic input impedance, the aortic blood flow on a beat-to-beat basis is accurate enough to use in routine clinical practice. [58]

4.4. Blood pressure

The blood pressure belongs to the four main vital signs routinely measured. The others are body temperature, respiratory rate and pulse rate; the last two being covered already in the previous sections, and temperature measurements being discussed in **Section 4.9**. While the range of normal blood pressure varies with age, gender, and fitness status among other factors, approximate normal values have been found for all these subgroups. The necessary large data sets are given by a systolic and diastolic value. However, as with many vital signs, the blood pressure fluctuates throughout the day and can be influenced by the consumed food, exercise, sleep rhythm, and many other short-term factors. [98] These variations have to be taken into account when single measurements are performed, *e.g.* at a yearly check-up. Hence, a long-term measurement would result in a more reliable value averaged throughout a day, week, or even longer. With these, the value for each individual can be averaged and evaluation is more representative. Abnormally low blood pressure values are called hypotension, the abnormally high ones hypertension.

In the standard upper arm sphygmomanometer measurement, the blood pressure is determined by an occlusion, which stops the blood flow. Complete occlusion can be checked acoustically with a stethoscope. Then, the pressure is slowly released until the blood starts flowing again (which leads to an acoustic noise), giving the upper value, the systolic pressure. The lower value, the diastolic pressure, is then received upon further release, at which the blood flows again unsuppressed and the noise disappears.

The mean arterial pressure (*MAP*) averages over the cardiac cycle and is given by the cardiac output (*CO*), the systemic vascular resistance (*SVR*) – determined by viscosity of blood, vessel radius, smoothness and length – and central venous pressure (*CVP*). While these values are not easily measured, the mean arterial pressure can be estimated by the upper (systolic) and lower (diastolic) blood pressure values.

(8)

$$\mathrm{MAP} = (\mathrm{CO} * \mathrm{SVR}) + \mathrm{CVP}$$

$$\cong P_{dias} + \frac{1}{3}\left(P_{sys} - P_{dias}\right)$$

Another value that has received interest is the pulse pressure (PP), taking the difference between the diastolic and systolic value. This relation depends on the stroke volume of the heart, the compliance of the aorta and the flow resistance. It has been shown that it correlates with the risk of a heart attack. [99] Hence, systolic and diastolic values are linked being an indicator for risk patient groups.

For newly developed devices, the accuracy has to be at least at the same level as for current devices. Furthermore, it should provide easy handling under long-term conditions. The accuracy is *e.g.* defined by the AAMI (Association for the Advancement of Medical Instrumentation): Mean values have to lie within ±5 mmHg and the standard deviations within ±8 mmHg. [100] Comfort in blood pressure management could include a cuffless version for providing a fast and stress-free hemodynamic evaluation. A proposed method is a pressure waveform monitor. [82d] The concept includes a fiber Bragg twin-grating Fabry-Perot interferometer. It can record the strain from the blood pressure applied to the artery wall, if the artery is close to the surface. The reflection spectra from the two Bragg gratings then show the usual reflection spectra forming an envelope as well as a cosinusoidal modulation due to interference between the reflection beams. For strain-induced changes to be visible, the distance between the two gratings should be several times the length of each grating. The

system is contained in a cuff to keep the gratings in place but it does not require inflation. The concepted set-up is seen in **Figure 8**, to which a feedback loop could be added. For this feedback, a wavelength change is induced proportional to the grating period increase due to thermal expansion. [82d]

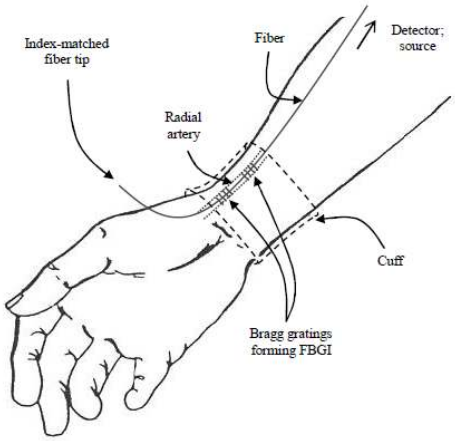

Figure 8: Blood pressure measurement with a fiber Bragg twin-grating Fabry-Perot interferometer – schematic [82d] , reproduced with permission by ©2005 SPIE.

Another approach to monitor the blood pressure continuously is a system using pulse oximetry (PO). [101] From the analysis, the diastolic, systolic, and mean arterial pressures were obtained. A large group of subjects requiring invasive blood pressure monitoring was used as a training cohort while a smaller group was used for validation after initial data acquisition and calibration. The algorithm was set up to build a probabilistic model of observed and hidden variables. Unfortunately, the researchers concluded that the large intrinsic variability of the blood pressure leads to lower precision than current commercial systems. [101] This limits the applicability not allowing for clinical tests yet.

4.5. Blood – Its flow, perfusion of tissues, hemoglobin volume and saturation of oxygen in tissue and arteries

Blood is the carrier of all nutrients through the body and the heart as its motor influences many paramerters affecting health. Such, the total blood volume, the oxygen carrying capacity and the return rate to the heart determine cardiac output, microcirculatory perfusion, and tissue oxygenation. The splanchnic circulation *e.g.* acts as a buffer in cases of depletion or expansion of the intravascular volume. [102] As oxygen is extremely important for the body and the functioning of the organs, continuous non-invasive oxygen saturation measurements have a huge market potential. After the uptake of oxygen through the lungs, it is transported in the blood through the body; either dissolved (reaching 0.28 % in normal conditions) or bound to the hemoglobin. Aoyagi, one of the first researchers for measuring the arterial oxygen saturation, has stated in 2003 that eventually each patient dies of mal-supply of oxygen to the heart or brain. Hence, a real-time, reliable, robust monitoring system for oxygen transport by blood is essential. [51]

Additionally to the total content of oxygen in the blood, cardiac output and arterial O_2 content are determinants for the well-being. To measure the partial pressure of oxygen in the alveoles and arteries, a complete look at the breathing cycle has to be done. For vastly different values of alveolar and arterial partial oxygen pressures, oxygen diffusion can be complicated. The decrease in partial pressure of air at inhalation already gives information on the capabilities in respiratory exchange of oxygen. The decrease of oxygen pressure into the body is called oxygen cascade and depends on humidification and respiratory exchange ratio. It contributes to the driving force of oxygen towards the cell mitochondria. [103] Oxygen delivery is defined as the quantity of oxygen delivered per minute to all organs depending on the cardiac output, the hemoglobin concentration, the arterial oxygen saturation, as well as the arterial oxygen pressure. [103] Hence, oxygen delivery is not only dependent on the variability of each individual but also on the momentary and long-term environment. In situations of increased oxygen demand, reduced oxygen supply and thermoregulation needs, stress in the oxygen delivery system occurs. This stress can then lead to an adapted circulatory regulation with the

central organs requiring the centralization of blood for minimum maintenance. The blood volume is then restrained to the torso and brain due to vasoconstriction of the peripheral vascular system. [102]

Typically, the oxygen saturation is measured in transmission mode. Hence, only thin body parts are feasible such as fingers or ear lobes. For these, fingers as part of the extremities might impede reliable values in case of blood centralization (primary brain perfusion maintenance). To allow light-opaque measurement sites, reflective pulse oximetry is favorable. [83] However, due to the drastically different output for the LED current or AC/DC-relation, the sensor interface has to be customized. [96] A summary of a study comparing the different techniques LDF, NIRS-HbT, and TVI (as discussed in **Section 2** to measure blood perfusion) can be seen in **Figure 9**. [50] The response to the different wavelengths was noticeable, especially in occlusion of the arm. Such, LDI showed no response while both NIRS and TVI showed a strong variation from the base line. Furthermore, a difference in response for subjects with varying melanin content in the skin was noted. [50]

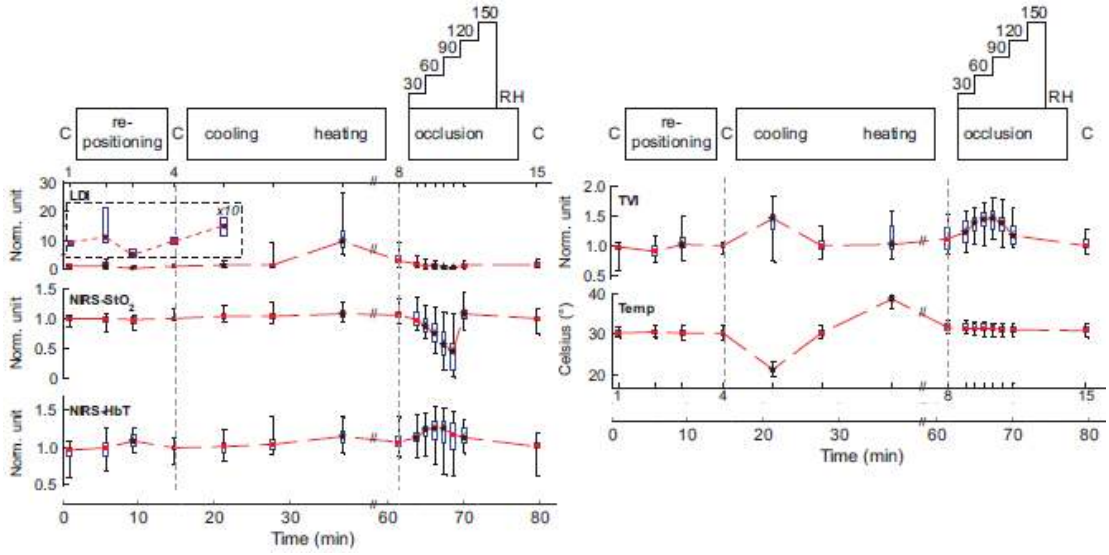

Figure 9: Responses of various non-invasive measurement techniques to different confounders in set-up. From top down: Measurement schematics, and results for LDI, NIRS-StO_2, NIRS-HbT, TVI, temperature respectively. The exact measurement set-up can be reread in Svanberg et al.'s experimental section (2011). [50] , reproduced with permission by ©2011 NRC Healthcare Press.

Applying NIRS for the monitoring of the oxygen content, muscle regions are possible measuring sites. For NIRS, the active muscle volume does not have to be determined. [104] Adding to the parameter of oxygen delivery, the hemoglobin content can be logged as well. While the hemoglobin concentration usually does not change fast, monitoring is not required but the added real-time information of sudden drops can indicate a bleeding. These drops in concentration arise as red blood cells are slower replaced than at which speed blood volume is shifted from other compartments of the body. A further correlation was found between abnormal tissue oxygen saturation values and requirement of lifesaving interventions. [105] Nevertheless, further calibration is necessary to exclude normal variations due to tissue type and the type of exercise. These influence the blood flow and thus change the response of the sensor. [106]

For choosing the wavelengths that are used in the measurement, the absorption of oxygenated and deoxygenated blood has to be evaluated. The relation of the two is then derived from a calibration curve. [107] The measured values are matched with known levels of tissue saturation. [50] Then, the oxygen saturation (SpO_2 *[%]*) can be calculated in later experiments from **Equation (9)** with difference of the signals for oxygenated hemoglobin (ΔO_2Hb) and deoxygenated hemoglobin (ΔHHb). While scattering may influence the measured values, the chosen wavelengths should not be isosbestic points in the oxy-Hb and deoxy-Hb absorption spectra. At these points the absorption properties are equal, thus not allowing for the calculation of oxygen saturation levels. [61b]

(9)

$$SpO_2 = \frac{\Delta O_2Hb}{\Delta O_2Hb + \Delta HHb} * 100\ \%$$

The blood flow can easily be recorded with PPG. However, during strong movements, the signal is hidden in artifacts. To suppress the movement artifacts, longer time ranges need to be evaluated to determine the natural range of blood flow. With knowledge of the normal

variations – the base line – , larger deviations in blood flow can be ascribed to *e.g.* increased heart rate during exercise. [54b]

While many parameters can be measured, artifacts can impede the interpretation of data. These artifacts from both external and internal influences are reduced in constant measurement surroundings. The state of the venous system plays an important role (*e.g.* pressure effects and congestion). Furthermore, the precise composition of the blood and tissue, such as bilirubin content due to absorption in the visible range, and hemoglobin variants affect the measurement as well as the positioning and the type of the sensor, ambient light, the temperature, and the motion of the patient. [107] For prevention of motion artifacts, again a multi-wavelength system was proposed still allowing for fast response times during the measurement. [51] For the evaluation of oxygen saturation in tissue, four wavelengths are necessary to deconvolute the impact of oxyhemoglobin, deoxyhemoglobin and CuA (the copper moiety of cytochrome c oxidase) in the absorption spectrum. [104] Adding further wavelengths, it was proposed to log carboxyhemoglobin, methemoglobin, total hemoglobin, and total oxygen content as well. [107] During measurements in reflection mode, the penetration depth depends on the light source and detector spacing.

Finally, an approach to reduce the error from methemoglobin and carboxyhemoglobin, a pulse oximeter was used with eight different wavelengths. Using multiple wavelengths (and advanced algorithms) allow the quantification of more hemoglobin derivatives in the blood due to the different absorption spectra. Focusing not only on the oxygenated and reduced hemoglobin in blood allows for diagnosis in cases of carbon monoxide poisoning or methemoglobinemia. [108] It has also been proposed to measure the complete spectrum over a wavelength range of 650-900 nm to improve the quantitative accuracy of total hemoglobin and hemoglobin oxygen saturation, while not being influenced extensively by water though with a sufficient penetration into tissue. [49, 109] A total-hemoglobinometer can be set up with inclusion of further wavelengths. Including the isosbestic wavelength, the effect of

hemoglobin oxygenation is reduced and the total hemoglobin concentration can be estimated in real time with fiber optic sensors. [61b, 110]

4.6. Pressure on tissue, and loading of cutaneous tissue layers

Pressure ulcers are dangerous injuries occurring with extended periods of lying or sitting in the same position. While tissue can withstand high pressures, inhomogeneously distributed stress can lead to impaired blood supply and to the decay of tissue. This degradation over an extended period prompts the onset deep-tissue injuries. [111] Also, occlusion of the lymphatic system has been mentioned as a potential danger during excessive epidermal loading. [62] It has been proposed to set a maximum pressure value to 4.3 kPa, the typical capillary blood pressure. With this maximum value, the microvasculature can withstand the external pressure ensuring supply of oxygen and nutrients. [62] However, much higher values of pressure on human tissue not causing injuries have been reported suggesting an approach scaling the maximum load to the duration time by $t^{-4/3}$. Hence, higher loads are allowed as long as the time frame is reduced. [62] During evaluation, one has to keep in mind that perfusion of different tissue types is often supplied by the same arteries. Hence, the ceasing of sufficient blood flow of outer tissue layers may to some extent give indications on lower tissue areas.

For gaining understanding of the underlaying reasons for the occurrence of pressure ulcers, the pressure distribution is mapped. It gives an indication on which areas are permanently under higher loads and if pressure peaks are present. These pressure peaks are very important to relieve periodically, as has been shown that a paraplegic patient's weight strongly lies on single protuberances. [111-112] While pressure ulcers are most common at the ischial tuberosity, foot problems for diabetics as well as high socket loading for amputees may cause skin problems. [62] Hence, a real-time measurement could help to adjust treatment releasing

pressure and ensuring continuous blood flow. Furthermore, the assessment on blood flow is important for healing of burn injuries, transplantation of skin flaps and for arteriogenesis. [54b]

The etiology of pressure ulcers has not been clarified yet impeding appropriate treatment plan development. The relation of the mechanics of compressed tissue and interface pressure is still being studied. [55, 113] As part of that question, the differentiation between abrasive ulcers and deep-tissue injuries is not cleared. [112a] These lesions grow either bottom-up or top-down, highly depending each patient, often also varying in ulcer depth. For instance, tissue layers are affected differently by compression during sitting or lying partially due to the changing inherent muscle tension. [111] Claudication can also be seen in patients with arterial lesions. These patients run much higher risk of developing tissue necrosis and also pressure ulcer.

To observe blood flow at several depths, photoplethysmography (PPG) and Laser Doppler flowmetry (LDF) as well as NIRS can be used for evaluating the pressure-related ceasing of blood flow. [55] Perfusion scales linearly with the velocity and the concentration of moving red blood cells. The exact set-up can vary greatly, though, also for this application, a multiplexing approach allows for transmitting the signals back to the photodiode. [53]

Additional information can be found with not only logging blood flow but pressure levels, *e.g.* on the mattress from the patient's body weight. While the relation between body mass index (BMI) and pressure ulcer development is still being discussed, it is clear that excessive weight on small areas has to be prevented. [112a] An important prerequisite for this application is the smoothness and flexibility of the pressure sensing system to not cause the build-up of an ulcer itself. [84f] Due to the small size of optical fibers, this requirement can theoretically be fulfilled. Geometrically, different approaches for measuring the pressure with FBGs have been used. A network matrix with crossings of OFs has been used as well as parallel strands of sensors. [114] Transferably to fiber optics, an electronic solution has been suggested for detecting the load position. [115] When fibers are introduced into a textile, the load can be logged *vs.* optical output. From the time delay and the change in optical output, the direction of the fiber in

relation to the strain can be read. [116] Additionally, depending on into which material the FBG is introduced – the response shows a hysteresis curve. [117] There are two different approaches for assessing the pressure instead of with FBGs: Intensity-modulated and phase-modulated sensing. Both depend on the total light level losses with either relating the displacement or the phase change of a coherent light beam to the applied pressure. For FBG sensors, the pressure is evaluated independently of the overall light level but the sensor is cross-sensitive to strain and temperature changes. [84e] To conclude, FBG sensors for pressure applications show many advantages. They are reliable in electromagnetic fields as well as are able to withstand a wide range of loads.

A method for reconstruction of fiber architecture in the body exemplarily shows the advantage of immunity to electromagnetic fields. The reconstruction mechanism included an indenter and FBG force sensor in combination with a SPAMM (spatial modulation of the magnetization), and an anatomical and diffusion tensor MRI. [84a] Finally, indentation force, tissue deformation and muscle tissue fiber architecture were received to produce a differentiated finite element (FE) model as can be seen in **Figure 10**.

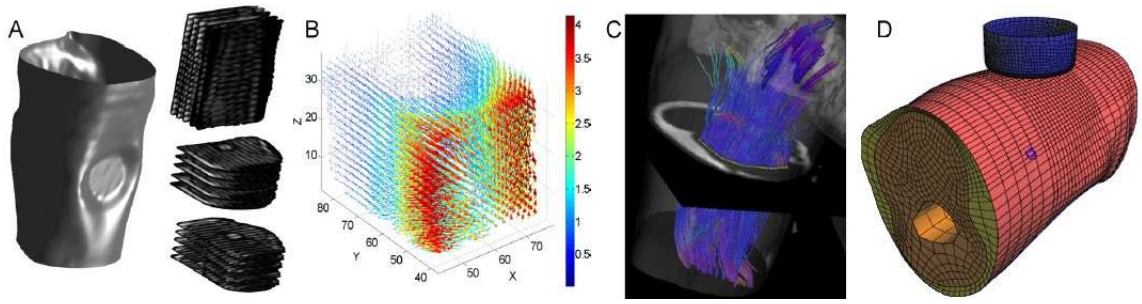

Figure 10: (A) Iso-surfaces in MRI for the indentation of a volunteer's arm, (B) 3D deformation measurement, (C) Measurement of the muscle tissue fiber architecture of the same arm (D) Detailed FE model with indenter model in blue derived from the combined measurements as well as anatomical MRI data [84a] , reproduced with permission by ©2012 IPEM, published by Elsevier Ltd.

Finally, their multiplexing ability leads to fewer sensors and, thus, less wiring. However, the maximum number of sensors is not only determined by the wavelengths able to be processed but is also determined by the distance to the detector. [84e] Furthermore, before usage, the system has to be calibrated, covering at least the range present in application.

The implementation of a sensing "skin" for prostheses is a long-term improvement for patients. Pressure sensing through normal forces opens the area of tactile sensing. [35, 115, 118] There, skin has to be divided into two groups: The first has a low spatial resolution, comparable to the skin of the body, the second on the other hand shows good spatial resolution, mimicking the skin of the finger. Both show good sensitivity. For these applications, the flexibility of optical fibers is of benefit again. In a prototype set-up, a FBG has been used, embedded in polydimethylsiloxane (PDMS) serving as a transducer. Due to the non-linear behavior of PDMS, however, the Bragg wavelength change also shows a non-linear response to applied forces. However, for a bridge-type taxel – a touch-sensitive amplifiying module – , the relationship was linear and not showing hysteresis. [35]

4.7. Shear stress on and in tissues

Shear stress on human tissue can cause significant injuries due to the different mechanical properties of tissue types. The monitoring of shear stress is especially important for prone to soft tissue injuries such as those often occurring with diabetes mellitus. Additionally, stress evaluation on prosthetic-body interfaces is important for improved comfort of amputees. [5a, 62, 84b, 84g]

For shear measurements, FBG sensors are used to measure axial strain via their output wavelength shift. However, to assess shear stress on the active surface, the FBG cannot pick up the axial strain from the same surface. A pre-tensioned FBG optical fiber spanning a disk-

like structure diagonally can give information on the strain in both directions along the axis. [84b] The schematic for this set-up is shown in **Figure 11**. Shear is evaluated by correlating the wavelength shift with displacement δ at a given height of the disk. Two approaches have been used additionally to correct for zero direction of the strain: Either using two FBG sensors in the disk-structure, or using two or more stacked pressure sensing sheets (**Section 0**). [84f, 84g] For both approaches a maximum deflection is given. For the disk, the maximum elongation of the FBG is determining while the pressure sheets' resolution is restricted by the grating pitch. A higher resolution could be obtained by additional pressure sheet layers.

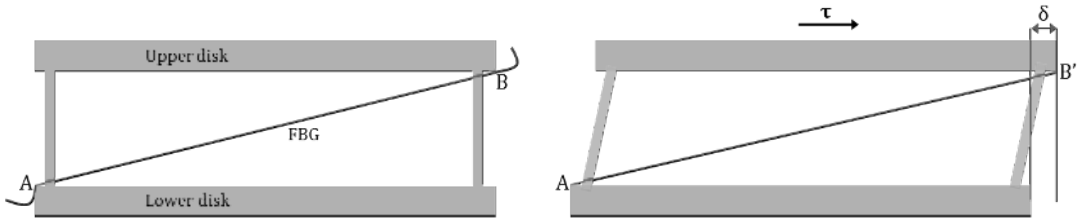

Figure 11: (left) Side view of the sensor consisting of lower and upper disk, and FBG, (right) Shear deformation of the sensor. The diagonally-placed FBG measures the strain on the upper surface. Adapted from A. V. Koulaxouzidis, V. C. Roberts, M. J. Holmes, V. A. Handerek, presented at the Applications of Optical Fiber Sensor, Glasgow, UK, 2000. [84b]

Research is currently going on on the pressure sensing sheets as part of an EU-project called SmartSocket. A schematic can be seen in **Figure 12 (left)**. A market-ready solution was also developed by Bioimerosin Laboratories SA (Thessaloniki, Greece). The concept is depicted in **Figure 12 (right)**. First tests in prosthetic sockets show that the FBG sensor has to be level with the socket to prevent additional stress on the patient's skin during pressure measurements. [5a, 119]

For long-term measurements, the approaches using the prerequisite of constant temperature have to be adjusted. Especially for patients with developed ulcers or foot tissue necrosis, the humidity and temperature levels may rise over the day. [84b]

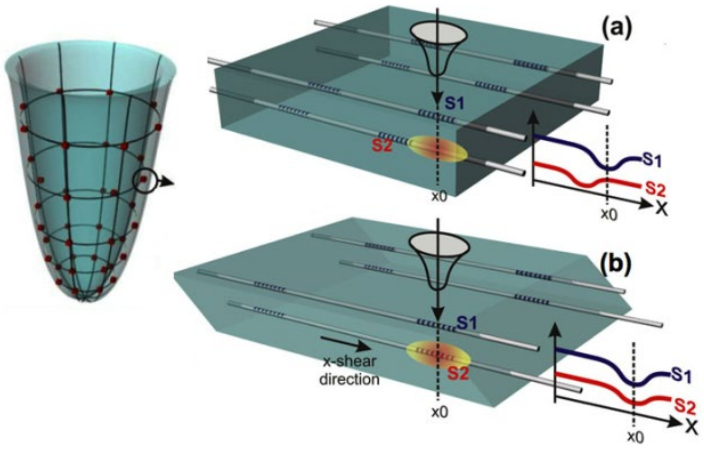

Figure 12: (left) Pressure sensing sheet to line a prosthetic socket for strain and pressure measurement with optical fibers, (right) Pressure and strain sensing concept: Orientation of the fibers is perpendicular for overlapping pressure spots while the strain is measured with several layers of FBG [120].

Fiber Bragg gratings enable measurements also for shear stresses. Having quantifiable data allows researchers and engineers to customize an optimum fit and to minimize shearing injuries.

4.8. Mobility and Gait analysis

Measuring the gait and joint movement of patients is a very important aspect of tracking the progress in accident rehabilitation. Also, illnesses such as cerebral palsy, Parkinson's disease or neuromuscular disorders necessitate gait analysis for designing a treatment plan. The entire joint movement sequence has to be analyzed by means of graphical real-time output. Thus, a high-sensitivity sensor such as a FBG optical fiber is needed. The gratings are introduced as described in **Section 2.1** and the bent joint is correlated with the shift in the Bragg wavelength. The moving joint generates axial strain on the FBG, effectively changing the grating pitch. For reliable measurements, the sensor has to be attached to the body above and below the joint, invariant of the movement of the subject. Errors can be caused by tendon creep, wrong calibration or skin movement artifacts. [19] Possible solutions to minimize the errors are pressure buttons attached to an elastic joint band or Velcro tapes strapped to the body. [84h, 121]

These options also allow the FBG sensor to lift from the joint when it is overextended. Hence both flexion and extension are transduced.

In the future, combining techniques presented in this section as well as in **0** and **4.7** may lead to mapping of biomechanical stresses, *e.g.* in the knee. The information obtained in extend of joint bending, plantar pressure and shear allows for biomechanical evaluation of gait. Additionally, forces acting on tendons, ligaments, and muscles around the joint can be estimated as well. From these, minimization of biomechanical stress is envisioned.

To reduce the tendon strain, the force incident angles are one of the most important factors. However, for individual biomechanical improvements, a universally fitting set-up proves to be difficult as size of joint and limb influence the measurements significantly. [121]

Another public health section regarding mobility is actimetry. It evaluates movement with the help of accelerometers. It has been found beneficial due to psychological aspects in human movement: The predominant reason for actimetric monitoring is a reduced muscle tonus of exercise-lacking elderly. The generally reduced strength and the fear of not being found after an accident then leads to further lack of movement which in turn increases the risk of injury. This vicious circle eventually leads to bed-bound patients, increasing the need for medical care drastically. The accelerometer-approach allows for tracking of movement, responding to both frequency and intensity. These systems have been minituarized as microelectronical systems (MEMS) but also accelerometers based on optical fibers systems are feasible. [13, 84d] The ability to combine analogue signals into a multiplexing signal of an FBG system, allows for both static and dynamic measurements. [84d] For this application to be successful, reliable alarm signals have to be triggered in case of a fall. Additionally, normal movements (*e.g.* daily activities of life, such as walking or sitting down) have to be filtered. In the case of return of movement after a fall has to be recognized as recovery so that intervention becomes unnecessary. [122] Thus, thresholds in acceleration have to be calibrated carefully. [122b] To

measure whole body movements, the accelerometer should be worn as close to the center of gravity of the body as possible to avoid false positives. Optimum site selection is evaluated for anterior/posterior and medial/lateral shifts. [122b]

Contributing to a decreased mobility can be balance deficiencies, often caused by loss of plantar cutaneous sensations. This relevant factor in balance control has been substituted with a tongue-based electrode. Plantar pressure mapping was used to monitor shifts from the median position. [123] While for this clinical test, an electronic system was used, pressure mapping has been done with optical fibers as discussed in **Section 0**. Using such unobtrusive systems can then lead to a safer feeling and finally with improving muscle tonus to a stronger confidence while moving. The patients' daily tasks are facilitated overall.

4.9. Temperature

Body-temperature is one of the most fundamental parameters reflecting health. Hyper- and hypothermia are very dangerous and variations from the norm over an extended period of time can mean harm to the functions of the body even on a long-term basis. Thermoregulation, both on the extremities and in the core, is hence very important. Consequently, it is desirable to monitor the temperature variations on-body over time.

One option for monitoring the temperature, the general equation of an FBG sensor (**Equation (6)**) can be simplified (**Equation (10)**), considering the other influences to be insignificant.

$$\Delta\lambda_{BT}[\mathrm{nm}] = \lambda_B(1+\xi)\Delta T \quad \textbf{(10)}$$

For the simplification to be true, a strain-free environment and a precise calibration has to be ensured during the measurements. The position of the FBG has to stay constant over the duration of the measurement. [44]

For these FBGs, electromagnetic immunity and relevant precision was shown. The accuracy stayed 0.05 °C in the range of 25-60 °C, with constant resolution under high magnetic fields (4.7 T). [41] For polymer optical fibers, resolutions of 0.1 °C have been achieved with a linearity of > 99 %. [25b] In comparison, liquid-in-glass thermometers can achieve a measurement uncertainty of ±0.01 °C in the range of 0 to 100 °C. [124] The magnitude of the temperature response is another important value. Such, the sensitivity for λ=800 nm and 1550 nm are ~6.8 pm/°C and ~13 pm/°C respectively for silica fibers. [34] The contribution in the shift is ~10 % for silica through thermal expansion while the remaining 90 % are determined by the change in refractive index of the fiber.

Advantageously to non-optical techniques, temperature changes can be logged simultaneously with other parameters using only one FBG-inscribed optical fiber. Additionally, they can be used in an environment with electromagnetic fields, and they can measure several locations along one fiber. For this, the fiber is inscribed with as many FBGs as needed. With each separate FBG, a different wavelength via their grating distance is reflected, thus covering all areas of interest. [42] Many further possible set-ups have been evaluated, among them, a polymer grating and a silica grating were combined to measure the strain and temperature more sensitively. [82e, 125]. As long as the polymer FBG shows a linear stress response, a combination of the two materials shows stronger sensitivity to strain. To differentiate between the parameter shifts, a matrix equation system can be set up. If the same number of parameters and equations exist, a unique solution can be found for the inverted linear equation system to receive a value for *e.g.* ΔT and $\Delta\varepsilon$ as the change in temperature and strain respectively. By adding further parameters, a superstructure fiber grating sensor can be developed, measuring several parameters simultaneously. [125] For such a optical fiber, the broadband and narrow-band loss peaks can *e.g.* be sensitive to temperature and axial strain while the transverse load induces a split in the broadband peak due to birefringence. [125]

While the FBG sensors are very sensitive, temperature can also be monitored with other methods of optical fiber technology. Interferometric configurations as well as temperature modulation sensors were used, all of which have to be calibrated or used in combination with a reference fiber. Constructing a sensor with a self-referencing technique can eliminate false readings due to fluctuations of the source or other unexpected effects. [25b] Thus, effects arising from the surrounding media, which might change in a practical application, are eliminated as well. Many interesting applications can arise from this possibility as well as research on the inclusion of other or even further parameters.

4.10. Electrolyte balance: Sweat, Humidity, and pH value

Medically, non-invasive fluid analyses from the human body are possible for urine, saliva, sweat, and tears. [126] Information can be gained through the chemical composition of these fluids at various stages of body metabolism and cleansing processes such as the nephrotic activity. [127] For a collection directly from a garment, sweat is the easiest and most unobtrusive to access. [126] With the developed technologies to transport the sweat from the skin to the outer garment layers, rerouting to a chemosensor is an option. Sweat contains among others sodium, potassium, urea, and lactate. The electrolyte balance can then be determined from the sweat composition to rule out pathological conditions. It also gives information about the activity, the hydration, environmental conditions, or mental status. Similarly, the pH value of a body is a fast indicator on whether an imbalance exists. Imbalances, as a consequence, either lead to alkalosis or acidosis. Both conditions are potentially life threatening and fast recognition is important. Closely related, the humidity value at the body indicates the sweating rate or, in case of wound monitoring, the process of wound healing. Determination of the occurrence of a systemic interference such as an inflammation during hemostasis becomes viable.

Sensing can be performed by several different approaches but for all of these the optical input has to be transduced into chemical recognition. The optodes (photonic sensors) nowadays determine molecules, pH, humidity level, temperature, and different biological species depending on the fiber configuration. A direct spectroscopic set-up allows to work with a series of different sensing geometries as can be seen in **Figure 13**. [73] The sensing film can be selected to match the application, *e.g.* a diblock copolymer allowing for sensing of various molecules by the specific polymer groups such as hydrophobic and hydrophilic parts. [128] Other approaches are evanescent wave sensors, in-fiber gratings, and interferometric sensors.

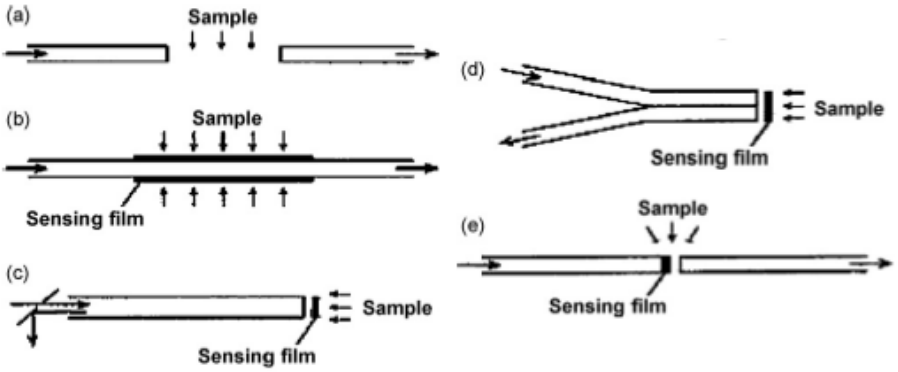

Figure 13: Sensing set-ups for optical fiber sensors in spectroscopic mode: (a) The sample lies between two optical fibers; one delivers the light to the sample, the other couples the light in after interaction with the sample, (b) The optical fiber is coated with a sensing film that allows for evaluation of the sample, (c) One optical fiber is used as an in- and out-coupling probe with a sensing film for the sample interaction, (d) and (e) are combinations of (a-c) [85], reproduced with permission by ©2008 Elsevier B.V.

As discussed in **Section 4.8**, humidity fiber Bragg grating sensors also use the adjusted equation introduced for strain and temperature changes (see **Equation (6)**). Such, the photoelastic constant ρ_e is related to the strain induced on the fiber by both the temperature and relative humidity. These two influences lead to polymer swelling which induces a strain in the fiber and consequently a change in FBG output. [84c] Additionally the termal expansion by temperature changes is taken into account. In the selection of the appropriate material, a sufficiently high response to humidity has to be ensured, while structural integrity is

maintained. Furthermore, the temperature dependency of the set-up can be erased by a second, blank optical fiber. A very extensive review on fiber-optic humidity measurements is given by Yeo, Sun, and Grattan (2008). [85] Long-period gratings (LPG) are more sensitive to refractive index changes than FBG. Generally, a chemical surrounding can be sensed due to interaction with the evanescent field. The refractive index of the chemical surrounding generates loss peaks in the transmission spectrum. This allows for sensing of molecules, as long as the loss peak lies within the refractive index range of 1.3-1.45. [41] Even more coupling possibilities open up with planar lightwave circuits. The LPGs can then allow for filtering, signal processing, and sensor functions. [129]

Humidity is not only measured with FBGs but also with specifically adjusted coatings on the optical fibers. Similarly, the photosensitivity can be adjusted flexibly with dopants, opening measuring capabilities in different wavelength windows. [45] With these fine-tunings, FBGs allow additional information, *e.g.* the pH. [84c] Optical detection of the pH is also possible with pH-sensitive dyes (pKa between 4 and 8), corresponding to the possible pH-range of sweat. This allows to monitor the color change. Similarly, color change has also been logged with an adjacent pH indicator or a fluorescent dye-doped micro-structured POF. [33, 126, 130] In terms of enhancing the response to the target molecule, core/shell nanoparticles have been used in a pre-clinical test to amplify the fluorescence behavior. [131]

Organic molecules can also be sensed with Surface-enhanced Raman scattering (SERS). Nanorod-coated optical fiber tips provide a portable mean of molecule identification. The electromagnetic properties are tuned with tapering the fiber and adjusting the shape of the particles. [132] While a prove of principle of the method was demonstrated, the signal-to-noise ratio has to be improved because identification of the fluorescence signals and distinction from the SERS and the background signal was shown to be demanding. [132]

For the same analyte molecules, Rhodamine 6G – in distilled water –, photoacoustic spectroscopy was used for the detection of chemical concentration (1000-10’000 ppm),

temperature and flow speed of the liquid. [133] Nevertheless, to receive the desired sensitivity level, the chemicals were enclosed in a cylinder. Therefore, for *e.g.* real-time sweat analysis on-body, a solution has to be found for noise-reduction and acoustic detection. [133]

Alternatively, on-fiber sensors can visualize changes due to an exchange of cladding in a small section of the fiber. This section then acts as the sensing element due to careful selection of the replacing analyte-sensitive material. The selection also insures that the target analyte is detected in the range covered by the application. Evaluation of the output is done in relation to the defined input power. [134]

Further technologies for fiber sensing include surface plasmon resonance (SPR) and photonic crystal fiber (PCF) technologies. SPR shows very high sensitivity as a change in the boundary condition alters the coupling condition between light wave and surface plasmon polariton. With the altered coupling, the intensity of guided light in the fiber changes as well. However, the SPR requires the deposition of a metal layer onto the core which leads to the possibility of an electromagnetic interference in some environments. PCF on the other hand utilizes a periodic dielectric structure with an introduced defect to receive a sharp transmission peak. A peak shift indicates a change in the environment. [135] Liquid-core PCFs could offer interesting possibilities for evaluation of fluids through their optical properties. [46]

Additionally, biosensors from planar waveguides show very good sensitivity. Often, the changes in the surrounding can be sensed, labeling on the surface of *e.g.* polymer chip is necessary though for surface binding sensing. [136] A relatively new development are label-free interferometer biosensors which also use the evanescent field for sensing their surrounding as also described in the following paragraph. [137] Depending on the set-up of the waveguide, the traveling depth of the evanescent wave can be changed. Inclusion of an interferometer structure (*e.g.* in a reference arm of the waveguide) leads to an interference signal proportional to the change in refractive index in the surrounding of the waveguide. The

review by Kozma, Kel, Ehrentreich-Förster, Stamm, and Bier (2014) includes a good differentiation of the sensing principles of the currently used interferometers. [137]

Multimaterial fibers produced from optical-fiber drawing show also interesting controllable electric and magnetic properties. They include several functional components. Co-drawing of metals, semiconductors, and insulators leads to optoelectronic and thermal opportunities. [15]

The evanescent wave is created due to interferences between incident and reflected signal. A standing wave is created extending into the cladding region, decaying exponentially. [85] To increase the penetration depth of the evanescent field, the fiber can generally be adjusted with tapering, bending, and launch angle as well as with the wavelength used. [138] Tapered fibers have the advantage that the evanescent field passes through the cladding to a higher percentage as they, geometrically, are local reductions in diameter of both core and cladding. Similarly to the refractive index profile in the fiber's cross section plane, they can be formed as a gradual decrease, a step-wise reduction or a single, abrupt step along the fiber. [139] Thus, tapers use the evanescent field characteristics to achieve higher specific sensitivities comparable to LPGs. Common production techniques for tapers include heat-pulling as well as chemical etching. During the production with chemical etching, the tapering can be monitored by measuring the transmitted power or effective numerical aperture. [139] The changes of the surrounding refractive index influence the difference between refractive index of "cladding" (external medium) and "core" (core and cladding in the tapered region). [140] In the tapered region, light propagation spreads to the cladding as it – with changes of the normalized frequency for both core and cladding – is no longer guided by the core-cladding interface. Regarding the medical analysis potential, salinity measurements were conducted. [140] Similarly, a tapered fiber was used for the determination of bacteria growth. [141] This method can allow rapid determination of bacteria presence in the proximity of the fiber. Additionally, further small-volume measurements have been conducted with fiber based refractive index sensors (FBRIS). An extensive list has been published by Zibaii, Kazemi,

Latifi, Azar, Hosseini, and Ghezelaiagh (2010). [141] Another compilation of evanescent biosensors was done by Leung, Shankar, and Mutharasan (2007) compiled an overview of evasnescent biosensors. [138] There, it was shown that tapered POFs respond differently to different types of cells. The response results among others from the changing refractive index of the higher concentrated cell solutions. [142] However, the response can also vary with the size difference of cells as well as evanescent field absorption, fluorescence and surface plasmon resonance. [138] Hence, in a true biological environment – with many different cells present at any point – a differentiation may be impossible. In such a case, an optical fiber that only shows a response for one cell type might be preferential. Nevertheless, the sensors can detect low concentrations of analyte and if improved in terms of selectivity, could detect specific cells.

Showing that these applications of on-body sensing are currently of great interest, an EU-funded project called BIOTEX was performed to develop a physiological supervision system. The chemical composition of sweat was of heightened interest in this project. The project included real-time measurements of sweat rate, ECG, respiration, and blood oxygenation. These sensors were distributed over the body to form a multi-sensor network. [143]

Finally, wound monitoring is possible with PPG signals as wounds require perfusion of the surrounding tissue to heal. [113a] Hence, showing the pulsatile character throughout the healing process, or the loss of pulsatility can indicate wound healing success. [58]

5. Wearable systems

For reaching the goal of continuously measuring vital parameters of a patient, the wearability of the system is of crucial importance. A reliable, safe and user-friendly monitoring device has to be ensured for a successful introduction to the market. Furthermore, the patient should be disturbed as little as possible by the monitoring system. [144] The components should

additionally be unobtrusive for the protection of privacy. Comfort, as mentioned in the introduction, is an important criterion as discomfort will lead to rejection of the proposed system. A smooth inclusion of the fibers into the garment is vital. For this, optical fibers prove to be advantageous due to many industrially available techniques to integrate them into a textile. The produced textiles are light-weight and show flexibility. Thus, they are suitable for long-term monitoring devices. For comfort, parameters such as yarn hairiness, unevenness and the number of faults play an important role. [145] In sweat collection, the fluid transport characteristics play an important role. [127] Furthermore, the number of loops, the wavelength and the effective extension of the fabric can optimize the signal quality drastically. In the European FP7 project OFSETH, the influence of these parameters for macro-bending sensors were summarized. Such the relation between loops, elongation and wavelength can be logged leading to higher or lower light intensities. [91]

Using optical fiber in garments requires for the fibers to have contact with the skin as well as being able to deliver light to the tissue. Another parameter for the feasibility is thus the luminosity of the fabric. It is determined by the material and diameter of the polymer optical fibers, the curvature of the fibers in the fabric, the fabric's yarn density and the corresponding light source. [146] Furthermore, treatment of the fibers before or after completion of the fabric can alter the light properties. Measures to increase the lateral light emission are sandblasting or chemical etching as well as notching and surface abrasion. [9b]

5.1. Integration of fibers into a textile

When integrating fibers, it is very important to consider the resulting properties of the fabric. Comparing to polymeric optical fibers, the resulting flexibility in electronic elements is a bottleneck. To establish a flexible electronic fabric, devices have been mounted onto flexible plastic strips which are then woven into the textile. This approach, however, necessitates

perpendicular connections with conductive yarn. [52, 147] While conductive yarns can now be woven and knitted which allows appropriate textile integration, the inclusion of electronic elements is difficult. Thus, they have been embedded in a flexible and wearable plastic to make them stretchable and washable for making long-term home usage imaginable. [148] Polymer optical fibers show a clear advantage for textile integration: The flexibility of the optical fiber can be matched to the yarns' flexibility resulting in a balanced fabric which maintains the homogeneity of the entire textile. For weaving, the selection of the yarn material is thus often influenced by the single fiber's mechanical properties. [146b] Nevertheless, the combination of fibers and yarns and weaving type can result in largely different properties.

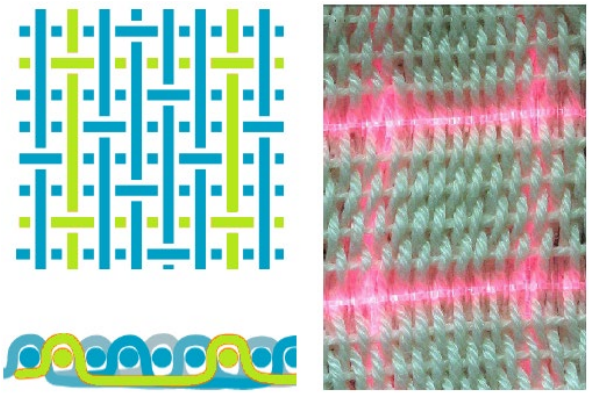

Figure 14: 4/1-twill with top view and cross section (both left) as well as produced prototype from silicone POF and cotton multifilament fibers (right). The parallel optical fibers are at a distance of 15 mm from each other. [114]

The bending situation in *e.g.* a Jacquard fabric has been simulated. There, the theoretical side-luminance can be related to both bending radius and weaving style. [146b] For the simulations of the side-luminance, the radius of curvature of the optical fiber is very important (as discussed in **Section 2.1**). The varying final fabric thickness h and the period of the optical fiber crossing p result in drastically different radii of curvature of the optical fibers: For a satin weave 4 and 8 (the weft yarn is alternatingly 4 respectively 8 times above and then once below the warp yarn) at the same thickness, the radius quadruples (from **Equation (11)** [149]).

(11)

$$r = \frac{h}{4} + \frac{p^2}{16h} \approx \frac{p^2}{16h}$$

In weaving, the assigned weft and warp threads are interlaced with each other in a produced fabric, as *e.g.* in an 4/1-twill weave (**Figure 14 (left)**). [146a] The twill *e.g.* shows a characteristic diagonal pattern. To produce a fabric, the warp threads are moved up and down by shafts to allow for introduction of the weft threads. [147] For differing materials for the two yarns, tensioning has to be matched. [9b, 150] The assignment influences the final properties.

Finally, the weave pattern not only has to provide a good spatial resolution during *e.g.* compression but also not to show drift, a slow change in response to the same stimulus. When optical fibers are partially used for both weft and warp directions, the drift has to be assessed for both fiber directions as well as for the light coupling between the fibers at intersections. [114] For the designed pressure sensor (as seen in **Figure 14 (right)**), the characteristic flexibility of the textile was kept and touch-sensing was achieved with a lateral resolution of 10 mm. Other groups have worked on assuring homogeneity of lateral light out-coupling with the fabric's medical potential in mind. [151] A medical application for a homogeneous lighting fabric is phototherapy. The luminance has to be kept constant over the entire area of the fabric to ensure uniform treatment. A textile light diffuser was produced with different satin weave patterns along the fiber thus increasing the bend radius with distance from the light source. This optimizes the out-coupling with the intensity decay along the fiber and leads to a homogeneous and flexible light diffuser. [152] Hence, the weaving pattern can be used to adjust light out-coupling over distance. Regarding the maximum side-emission of light, cracks and post-weave treatment were considered, but noted that the transmission distance decreased substantially. [150]

Additionally, for a successful usage of the fibers in a textile, the efficiency in light delivery has to be efficient. The light intensity detected from the textile over the light intensity from

the source gives the efficiency ratio. [149] Hence, to increase resilience and prevent losses, weaving of cotton fibers around a polymer optical fiber has been tested. It showed better mechanical properties and allowed for post-manufacturing into a textile with both power and hand loom. [153]

In embroidery, the optical fiber is sewn onto a substrate material. Hence, contrary to weaving or knitting, the fibers are introduced after the textile has been produced. This prevents a continuous macro-bending as observed in weaving or knitting. For light emission purposes, various configurations can be created as seen in **Figure 15**. For these embroidered structures one has to regard the anticipated force direction as denoted with *F* in the schematic. It is clearly visible that some of the structures are not feasible for all parameters discussed in **Section 4**. Effective light-emitting embroideries using arbitrarily twined fibers ("Schiffli") attached on a woven substrate have been tested, as depicted in **Figure 16**. However, the determination of the exact position and the number of bends is difficult. [146a] The "Schiffli" are very useful though as they emit much light in the loops while being protected from high pressures since the straight path of the optical fiber lies on the contrary side of the fabric as illustrated in **Figure 16**.

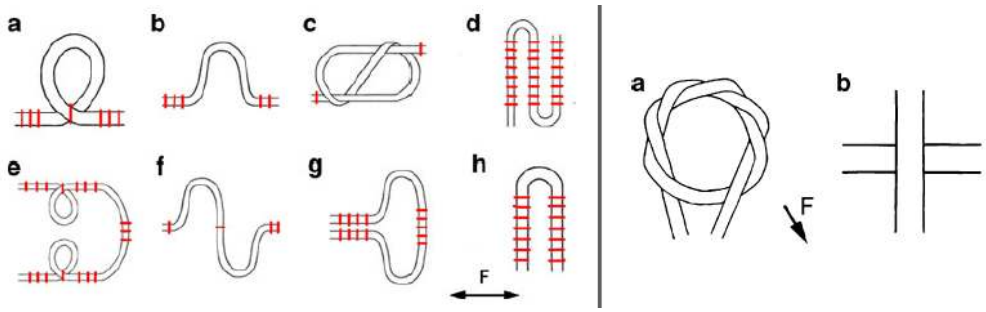

Figure 15: (left) Possible macro-bending sensor structures: a – loop, b – wave, c – eight, d – serpent, e – double loop, f – double wave, g – mirror wave, h – single serpent, (right) Micro-bending sensor structures: a – knot, b – cross [154], reproduced with permission by ©Springer-Verlag London Limited 2010.

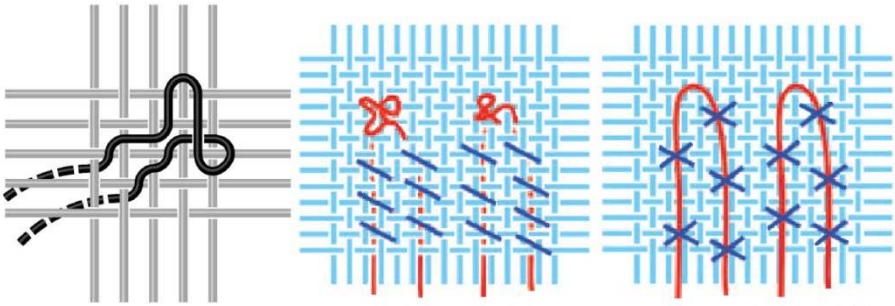

Figure 16: Embroidered structures – (left) two schematics of "Schiffli" of optical fiber. The fibers are lead on one side of the canvas, then thread through the fabric to produce random loops [146a, 155], reproduced with permission by ©2007 SPIE, (right) Soutage consists of a canvas (light blue fabric) with optical fibers (red) placed on one side of the canvas in a required shape while the stitches (dark blue) keep the structure in place. [146a]

Knitware has high potential for lighting objects with complex geometry due to the good drapeability. [146a] To optimize the fabric, different knitting stitches can be tested which resulted in a variation of tightness for conductive yarn. Thus, a modification of the design for different applications is possible. [148c] These results give information also on possibilities for the usage of optical fibers. The introduction of pockets or tubular stitches also facilitates the placement of electronic devices. Depending on the fiber strength, the knitware needs to be tightened for a good contact. A zipper system was tested with conductive yarn which permitted higher comfort of the garment during non-measurement phases. [148c]

Concluding, integration of optical fibers into a textile is possible both with incorporation into as well as onto an existing fabric. Textile production parameters allow tuning of flexibility as well as light out-coupling. Hence, properties with the in textile processing allow for various interative methods for the optical fiber

5.2. Flexible hosts for optical fiber embedding

The applications for medical care with flexible sheets are determination of the breathing pattern, the cardiac frequency and temperature. [156] In a flexible sheet, these sensors are more robust to surrounding influences as well as reliable positioning and contouring of a monitored body part. [157] Their flexibility and drapeability for good contact and fold-avoidance on irregular surfaces are important to produce "artificial sensing skins". Embedding of optical fibers has lead to the development of new production methods. These can both protect the fibers from mechanical stresses as well as from chemicals. Mass production can be achieved by curing of the polymer after embedding, *e.g.* with UV polymerization. This method can be performed in large scale and can be adapted to a continuous line. The flexibility of the film can be adjusted due to the vast variety of the materials available nowadays.

For the production, a requirement is the compatibility or inertness to the fiber coating as well as the preservation of refractive index. Such, the grating wavelength of an FBG fiber has to be reassessed after curing due to possible contractions of the host polymer film. [119] When introduced into the flexible host, the geometry of the fibers has an influence on the sensing behaviour. The sensing response has to be calibrated and should only be influenced by one parameter, *e.g.* bending angle. The embedding can thus be adapted to the desired application. For medical solutions, biocompatibility has to be ensured as well. [18]

Differently to introducing a POF into a host, a polymer planar Bragg grating can be used as well. [158] The integrated grating can be stretched with the bulk PMMA and such show a response to compression or tension.

Showing the combined positive aspects of a sensing skin, the multiplexing ability of a single FBG fiber was used to cover the entire hand in the investigation of returning finger movement in rehabilitation. [157] The angle between finger phalanxes was reliably assessed. The exact position of the fiber was ensured by sewing the foil on top of a cloth glove which in turn ensured biocompatibilty and a comfortable skin climate. [159] While a multipoint operation of

a 2D sensor was verified with corresponding power loss calibration, a trial bed for pressure assessment was produced as part of a European research program. [84f, 160] These FBG sensors were introduced into a PDMS sheet. The sensing surface enabled the exact reading of the pressure distribution as the FBGs' positions were constant in spacing. Its set-up was discussed in **Section 4.7 - Shear stress**. Additionally to these examples, researchers have also suggested the embedment into a PMA (polymethylacrylate) tube as well as meandering fiber shapes (in *e.g.* silicone, PVC, PU or PMMA/EHMA) for creating an elastic sensing sheet. [18, 117, 156] While these were introduced into a preform, the connection of the two sheets (of *e.g.* PDMS) is also possible by plasma treatment. [161]

5.3. Practical aspects of wearable systems

Completing the wearable system is the last crucial part in the design of a wireless body sensor network. To assemble the wearable system, not only the fiber has to be part of the textile but also the corresponding signaling means. Thus, further important research foci of these wearable systems are among others the connection to the light source, signal transferring, data processing, and removal of artifacts. Challenges also include the range of transmission and low energy consumption. Prior to use, the integrated sensors are evaluated to verify whether the mechanical and optical properties were influenced by the integration process.

First, the optical fibers need to be connected to the light source. There, the cleavage conditions are important to not split the core from the cladding and to maximize the light coupling. One example for this is seen in **Figure 17**. Cleaving is influences by the sharpness of the blade and the blade's and fiber's temperature. Possibilities also include more expensive options such as UV laser cleaving as well as focused ion beam (FIB) milling. [74] It was found for a GI mPOF (Graded-index micro-structured POF) that the optimum cleavage temperature corresponds to the material's first peak in the loss modulus hence being influenced by the

material's viscoelastic properties. [74, 162] To connect fibers with different softening behaviors, fusion with good interfaces can become difficult. For these cases, the use of an elastomeric connector which matches with the refractive indeces and the diameters of core and cladding can help. [82e]

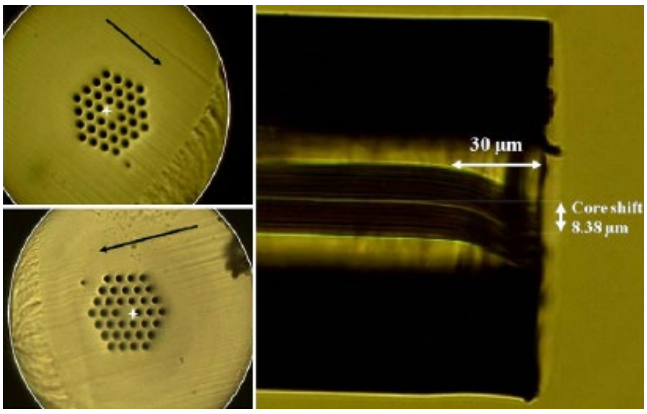

Figure 17: (left) Core shift dependence on cleaving direction at near-optimal temperature of the blade, (right) Microscope image of a cleaved fiber in cross-section is shown. Due to cutting, the core shifts inside the fiber leading to light loss. The core shift is 8.38 µm at the interface while misalignment starts 30 µm inside the fiber [74], reproduced with permission by ©2011 Elsevier B.V.

To transfer the data to a processor, a component for wireless transmission is necessary. These transmission means can be divided into three situations: off-, on- and in-body. Since this review focuses on non-invasive measurements, the third category is not covered. However, communication of the sensors to a data collector in proximity as well as between two or more sensors on-body can be necessary. [11] The different low-cost communication options feature different ranges, transmission rates and power consumption. Set-ups for specific situations (such as ultralow battery consumption or high data throughput) can be specialized as many options are available (e.g. Bluetooth or Zigbee). For all options, the battery life and thus power consumption is crucial and thus has to be minimized. [4, 163] The receiving end, or processing core, can be a computer or smartphones. [9a, 144] These can also generate emergency messages when necessary. [10b]

Having defined the exact use of the device, the obtained data has to be processed and interpreted. Generally, the resolution needs to be high enough and the signals from different optical sensing set-ups have to be separated. [54a, 114] If these conditions are fulfilled, several different further filtering techniques have been suggested. Such, motion artifacts arising during running were filtered with an adaptive technique for movement detection. [12b] Also described for an electronic solution, the accelerometer signal for the y-direction (the axes of the largest motion-induced displacement) was used as a reference to reduce motion artifacts in ECG. [7] Frequently, band-pass filters (*e.g.* Butterworth filters, the wavelet transform *à trous* algorithm (which introduces zeros/holes into the filters) or differential wavelet transform (DWT)) are applied. [164] The latter uses the concept of a multi-scale differential operator with which scattering effects are quenched and unwanted spectral variations are reduced by a smoothing function. [61b] For enhancement of the resolution in NIRS, a Wiener filter was considered for refocusing in vivo images, hence assuming time-invariant noise occurrence. [106] After receiving a smooth function, the data can be read.

Lastly, to receive medical device approval, the textile has to be safe for the patient to use. Therefore, the fiber sensors have to be sterilized to eliminate microorganisms and prevent later growth of bacteria on the textile. Sterilization of fibers can be classified into thermal or chemical treatment or irradiation. The choice of treatment is influenced by whether the sterilization method influences the fiber properties such as the median fracture strength or attenuation. Exemplarily, gamma rays should generally be avoided for optical fiber treatment. [165]

6. Conclusion and Outlook

Health monitoring based on polymer optical fibers is an ever-increasing field of research. Due to the technological advance of optical fiber sensors, complicated applications will become a reality. Extensive monitoring systems are conceived. For the introduction into homecare, the long-term monitoring systems need to have adequate material properties, feasibility in a continuous production and during implementation into fabrics. The reliability of the sensors has to be ensured and – at this point – further improved. Self-calibration is still a large issue due to the high variability of the optical properties of tissue. These reliable systems are, however, a necessity for a successful and large-scale market entrance. Yet, when these obstacles are overcome, the potential market is tremendous.

Material-wise, a further problem of fiber-based systems is the production of the fibers, especially of POFs. For the development of new fibers, high knowledge on polymer technology is crucial. To determine the small window for production parameters yielding reproducible, uniform fiber properties is time-consuming. Yet, once a set of parameters is found, a high-speed production of fibers is possible.

Further research and development is also decisive for the completion of the such systems, especially regarding the in- and out-coupling of light as well as data management which includes the transmission to a receiver. Light coupling still is a factor of instability, causing artifacts. Thus, more stable connections are desired. Furthermore, wireless solutions are the most convenient, for which battery life and receiving distance are crucial parameters. Additionally, these electronic components then have to be small and unobtrusive to maintain the positive aspects of optical fiber solutions. A solution of including the photodetector as on-chip sensing system of a polymer waveguide grating sensor is presented by Song, Xiao, Xie, and Seo (2013). [166] Fabrics are ideally suited for wearable devices due to the haptic, the moisture management, and the wearing acceptance. Fabrics including optical fibers have the advantage of possible long life-times due to high flexibility and elasticity. The challenges to integrate optical fibers into fabrics without influencing the properties of the fabric have been

identified and many ongoing activities try to improve the fusing and splicing. Thus, highly optimized sets of production and processing parameters are necessary for considerable reliability.

Finally, the real potential of optical fiber sensors is seen in applications and fields in which electronic counterparts are unsuitable. Those not only include diagnostic means (*e.g.* MRI) but also other biomedical appliances (*e.g.* pace maker). For any patients, a wearable, invisible, and comfortable monitoring device will allow for a more self-determined life and thus improve their quality of life substantially.

[1] WHO, *Ageing and life-course,* http://www.who.int/ageing/en/, **accessed October, 2013**
[2] O. Theou, T. D. Brothers, M. R. Rockwood, D. Haardt, A. Mitnitski, K. Rockwood, *Age Ageing* **2013**, *42*, 614.
[3] M. Chan, D. Estève, J.-Y. Fourniols, C. Escriba, E. Campo, *Artif. Intell. Med.* **2012**, *56*, 137.
[4] P. Jourand, H. De Clercq, R. Puers, *Sens. Actuators, A* **2010**, *161*, 288.
[5] a) E. Al-Fakih, N. A. A. Osman, F. R. M. Adikan, *Sensors (Switzerland)* **2012**, *12*, 12890; b) R. J. N. Helmer, D. Farrow, K. Ball, E. Phillips, A. Farouil, I. Blanchonette, *Procedia Eng.* **2011**, *13*, 513; c) R. J. N. Helmer, M. A. Mestrovic, K. Taylor, B. Philpot, D. Wilde, D. Farrow, *20th International Conference on Artificial Reality and Telexistence (ICAT2010), 1-3 December 2010, Adelaide, Australia* **2010**; d) J. McLaren, R. J. N. Helmer, S. L. Horne, I. Blanchonette, *Procedia Eng.* **2010**, *2*, 3041; e) C. D. Mackinnon, *Mov. Disord.* **2013**, *28*.
[6] W. Aeschimann, *Telemedizin im alpinismus - «hallo, ich habe ein problem!»,* NZZ, Neue Zürcher Zeitung, http://www.nzz.ch/lebensart/reisen-freizeit/hallo-ich-habe-ein-problem-1.18194101, **2013** accessed *2013-12-02*.
[7] Y.-D. Lee, W.-Y. Chung, *Sens. Actuators, B* **2009**, *140*, 390.
[8] P. Lukowicz, *Artif. Intell. Med.* **2008**, *42*, 95.
[9] a) F. Axisa, P. M. Schmitt, C. Gehin, G. Delhomme, E. McAdams, A. Dittmar, *Ieee Transactions on Information Technology in Biomedicine* **2005**, *9*, 325; b) J. Shen, X. M. Tao, D. Q. Ying, C. Y. Hui, G. F. Wang, *Text. Res. J.* **2013**, *83*, 730.
[10] a) V. Mishra, N. Singh, U. Tiwari, P. Kapur, *Sens. Actuators, A* **2011**, *167*, 279; b) A. Pantelopoulos, N. G. Bourbakis, *Ieee Transactions on Systems Man and Cybernetics Part C-Applications and Reviews* **2010**, *40*, 1.
[11] T. Yilmaz, R. Foster, Y. Hao, *Sensors* **2010**, *10*, 10837.
[12] a) T. Vervust, G. Buyle, F. Bossuyt, J. Vanfleteren, *J. Text. Inst.* **2012**, *103*, 1127; b) S. A. Santos, B. Venema, S. Leonhardt, *Acta Polytech.* **2012**, *52*, 80.
[13] E. T. McAdams, C. Gehin, N. Noury, C. Ramon, R. Nocua, B. Massot, A. Oliveira, A. Dittmar, C. D. Nugent, J. McLaughlin, in, 55 LNEE, Advances in Biomedical Sensing, Measurements, Instrumentation and Systems (Eds: S.C. Mukhopadhyay, A. Lay-Ekuakille), **2010**.
[14] S. J. Genuis, *Public Health* **2008**, *122*, 113.
[15] A. F. Abouraddy, M. Bayindir, G. Benoit, S. D. Hart, K. Kuriki, N. Orf, O. Shapira, F. Sorin, B. Temelkuran, Y. Fink, *Nat Mater* **2007**, *6*, 336.
[16] a) L. I. Hui, O. U. Jinping, *Procedia Engineering* **2011**, *14*, 753; b) Y. Koike, M. Asai, *NPG Asia Mater.* **2009**, *1*, 22; c) A. Kulkarni, J. Na, Y. J. Kim, S. Baik, T. Kim, *Opt. Fiber Technol.* **2009**, *15*, 131; d) A. F. M. Seyam, T. Hamouda, *J. Text. Inst.* **2013**, *104*, 892; e) F. Taffoni, D. Formica, P. Saccomandi, G. Di Pino, E. Schena, *Sensors (Switzerland)* **2013**, *13*, 14105.
[17] L. Bilro, N. Alberto, J. L. Pinto, R. Nogueira, *Sensors* **2012**, *12*, 12184.
[18] E. Ferraris, T. Van Gijseghem, C. Yan, B. Van Hoe, G. Van Steenberge, P. Van Daele, P. Dubruel, D. Reynaerts, Embedding of fibre optic sensors within flexible host, in: International Conferences on Multi-Material Micro Manufacture, 4M/International Conferences on Micro Manufacturing, ICOMM, Karlsruhe, 2009, pp. 351.
[19] P. Roriz, A. Ramos, J. L. Santos, J. A. Simões, *Photonic Sens.* **2012**, *2*, 315.
[20] N. A. Issa, C. V. K. Schmising, N. A. van Eijkelenborg, W. E. Padden, in *Optical fibers and sensors for medical applications v*, 5691 (Eds: I. Gannot), Spie-Int Soc Optical Engineering, Bellingham **2005**.
[21] J. Zubia, J. Arrue, *Opt. Fiber Technol.* **2001**, *7*, 101.
[22] A. F. Garito, J. Wang, R. Gao, *Science* **1998**, *281*, 962.
[23] O. Ziemann, in *Specialty optical fibers handbook*, (Eds: T.F.M. Alexis Méndez), Academic Press, **2007**.

[24] D. Donlagic, B. Lenardic, S. Rehman, in *Photonic Applications for Aerospace, Transportation, and Harsh Environment Iii* (Eds: A.A. Kazemi, N. Javahiraly, A.S. Panahi, S. Thibault, B.C. Kress), Bellingham **2012**.
[25] a) G. Durana, J. Zubia, J. Arrue, G. Aldabaldetreku, J. Mateo, *Appl. Opt.* **2003**, *42*, 997; b) A. T. Moraleda, C. V. García, J. Z. Zaballa, J. Arrue, *Sensors (Switzerland)* **2013**, *13*, 13076.
[26] A. Endruweit, A. C. Long, M. S. Johnson, *Smart Mater. Struct.* **2008**, *17*.
[27] M. A. Losada, I. Garces, J. Mateo, I. Salinas, J. Lou, J. Zubia, *J. Lightwave Technol.* **2002**, *20*, 1160.
[28] M. D. Feit, J. A. Fleck, *Appl. Opt.* **1980**, *19*, 1154.
[29] A. A. P. Boechat, D. Su, D. R. Hall, J. D. C. Jones, *Appl. Opt.* **1991**, *30*, 321.
[30] R. W. Smink, B. P. de Hon, A. G. Tijhuis, *J. Opt. Soc. Am. B* **2007**, *24*, 2610.
[31] J. Arrue, J. Zubia, G. Durana, J. Mateo, *IEEE J. Sel. Top. Quantum Electron.* **2001**, *7*, 836.
[32] M. Vadakke Matham, in *Optical waveguides, from theory to applied technologies*, (Eds: M. L. Calvo, V. Lakshminarayanan), CRC Press, Taylor & Francis Group, Boca Raton, FL, USA **2007**, Biomedical Fiber Optics.
[33] G. D. Peng, Z. Xiong, P. L. Chu, *Opt. Fiber Technol.* **1999**, *5*, 242.
[34] Y. J. Rao, *Meas. Sci. Technol.* **1997**, *8*, 355.
[35] J. S. Heo, J. H. Chung, J. J. Lee, *Sens. Actuators, A* **2006**, *126*, 312.
[36] A. D. Kersey, M. A. Davis, H. J. Patrick, M. LeBlanc, K. P. Koo, C. G. Askins, M. A. Putnam, E. J. Friebele, *J. Lightwave Technol.* **1997**, *15*, 1442.
[37] R. Kashyap, in, (Eds, Academic Press, Boston **2010**, Principles of Optical Fiber Grating Sensors.
[38] W. Yuan, A. Stefani, M. Bache, T. Jacobsen, B. Rose, N. Herholdt-Rasmussen, F. K. Nielsen, S. Andresen, O. B. Sørensen, K. S. Hansen, O. Bang, *Opt. Commun.* **2011**, *284*, 176.
[39] a) H. Y. Liu, H. B. Liu, G. D. Peng, *Opt. Commun.* **2005**, *251*, 37; b) Y. Luo, B. Yan, M. Li, X. Zhang, W. Wu, Q. Zhang, G.-D. Peng, *Opt. Fiber Technol.* **2011**, *17*, 201.
[40] D. X. Yang, J. Yu, X. Tao, H. Tam, *Mater. Sci. Eng., A* **2004**, *364*, 256.
[41] Y. J. Rao, *Opt. Laser Eng.* **1999**, *31*, 297.
[42] M. Matin, N. Hussain, R. Shoureshi, in *SPIE - The International Society for Optical Engineering* (Eds: K. M. Iftekharuddin, A.A.S. Awwal), San Diego, CA; United States **2005**.
[43] H. Y. Liu, H. B. Liu, G. D. Peng, P. L. Chu, *Opt. Commun.* **2006**, *266*, 132.
[44] J. Arata, S. Terakawa, H. Fujimoto, *Procedia CIRP* **2013**, *5*, 66.
[45] H. Y. Tam, C.-F. J. Pun, G. Zhou, X. Cheng, M. L. V. Tse, *Opt. Fiber Technol.* **2010**, *16*, 357.
[46] M. B. C. Cristiano, J. S. d. M. Christiano, M. d. S. Eliane, B. Alexandre, S. K. O. Jackson, F. Tilon, C. Giancarlo, R. V. Alfredo, H. B. C. Carlos, *Meas. Sci. Technol.* **2007**, *18*, 3075.
[47] A. D. Kersey, *Opt. Fiber Technol.* **1996**, *2*, 291.
[48] D. T. Delpy, M. Cope, *Philos. Trans. R. Soc., B* **1997**, *352*, 649.
[49] T. Hamaoka, K. K. McCully, V. Quaresima, K. Yamamoto, B. Chance, *BIOMEDO* **2007**, *12*.
[50] E. K. Svanberg, P. Wollmer, S. Andersson-Engels, J. Åkeson, *Appl. Physiol., Nutr., Metab.* **2011**, *36*, 946.
[51] T. Aoyagi, *Jour. Anesthesia* **2003**, *17*, 259.
[52] C. Zysset, N. Nasseri, L. Buthe, N. Munzenrieder, T. Kinkeldei, L. Petti, S. Kleiser, G. A. Salvatore, M. Wolf, G. Troster, *Opt. Express* **2013**, *21*, 3213.
[53] M. Hickey, P. A. Kyriacou, *J. Phys.: Conf. Ser.* **2007**, *85*.
[54] a) J. Hagblad, M. Folke, L. G. Lindberg, M. Linden, in *15th nordic-baltic conference on biomedical engineering and medical physics*, 34 (Eds: K. Dremstrup, S. Rees, O. Jensen),

Springer, New York **2011**; b) J. Hagblad, L. G. Lindberg, A. K. Andersson, S. Bergstrand, M. Lindgren, A. C. Ek, M. Folke, M. Linden, *Med Biol Eng Comput* **2010**, *48*, 415.
[55] S. Bergstrand, T. Lanne, A. C. Ek, L. G. Lindberg, M. Linden, M. Lindgren, *Microcirculation* **2010**, *17*, 311.
[56] J. Hagblad, M. Folke, L. G. Lindberg, M. Linden, *Physiol. Meas.* **2012**, *33*, 985.
[57] T. Binzoni, D. Tchernin, J. N. Hyacinthe, D. Van De Ville, J. Richiardi, *Physiol. Meas.* **2013**, *34*, N25.
[58] J. Allen, *Physiol. Meas.* **2007**, *28*, R1.
[59] J. Mateus, A. R. Hargens, *Physiol. Meas.* **2012**, *33*, 1027.
[60] J. Eichler, J. Knof, H. Lenz, *Radiat. Environ. Biophys.* **1977**, *14*, 239.
[61] a) R. R. Anderson, J. A. Parrish, *J. Invest. Dermatol.* **1981**, *77*, 13; b) P. Chen, B. Fernald, W. Lin, *Phys. Med. Biol.* **2011**, *56*, 3985.
[62] A. F. T. Mak, M. Zhang, E. W. C. Tam, in *Annual review of biomedical engineering, vol 12*, 12 (Eds: M.L. Yarmush, J.S. Duncan, M.L. Gray), Annual Reviews, Palo Alto, CA, USA **2010**.
[63] G. M. Palmer, C. Zhu, T. M. Breslin, F. Xu, K. W. Gilchrist, N. Ramanujam, *Appl. Opt.* **2006**, *45*, 1072.
[64] D. T. Delpy, M. Cope, P. Vanderzee, S. Arridge, S. Wray, J. Wyatt, *Phys. Med. Biol.* **1988**, *33*, 1433.
[65] J. M. Schmitt, G. Kumar, *Appl. Opt.* **1998**, *37*, 2788.
[66] A. N. Bashkatov, E. A. Genina, V. I. Kochubey, V. V. Tuchin, *J. Phys. D: Appl. Phys.* **2005**, *38*, 2543.
[67] W. J. Cui, C. Kumar, B. Chance, in *Time-Resolved Spectroscopy and Imaging of Tissues* (Eds: B. Chance), Bellingham, WA, USA **1991**.
[68] O. S. Khalil, S. J. Yeh, M. G. Lowery, X. Wu, C. F. Hanna, S. Kantor, T. W. Jeng, J. S. Kanger, R. A. Bolt, F. F. De Mul, *BIOMEDO* **2003**, *8*, 191.
[69] T. Fujimura, Y. Takagi, I. Sugano, Y. Sano, N. Yamaguchi, T. Kitahara, Y. Takema, R. L. Rizer, *Int. J. Cosmetic Sci.* **2011**, *33*, 566.
[70] a) Y. Li, *Ergonomics* **2005**, *48*, 234; b) R. Niedermann, R. M. Rossi, *Textile Research Journal* **2012**, *82*, 374; c) L. C. Gerhardt, V. Strässle, A. Lenz, N. D. Spencer, S. Derler, *J. R. Soc., Interface* **2008**, *5*, 1317.
[71] a) T. Fresvig, P. Ludvigsen, H. Steen, O. Reikerås, *Med. Eng. Phys.* **2008**, *30*, 104; b) M. Vilimek, *J. Biomech.* **2008**, *41, Supplement 1*, S511.
[72] a) R. He, P. J. A. Sazio, A. C. Peacock, N. Healy, J. R. Sparks, M. Krishnamurthi, V. Gopalan, J. V. Badding, *Nat. Photonics* **2012**, *6*, 174; b) M. Krehel, R. M. Rossi, G.-L. Bona, L. J. Scherer, *Sensors* **2013**, *13*, 11956; c) A. Marcinčin, *Prog. Polym. Sci.* **2002**, *27*, 853; d) J. Ballato, P. Dragic, *J. Am. Ceram. Soc.* **2013**, *96*, 2675.
[73] A. Harlin, H. Myllymäki, K. Grahn, *Autex Res. J.* **2002**, *2*, 132.
[74] A. Stefani, K. Nielsen, H. K. Rasmussen, O. Bang, *Opt. Commun.* **2012**, *285*, 1825.
[75] R. Hirose, M. Asai, A. Kondo, Y. Koike, *Appl. Opt.* **2008**, *47*, 4177.
[76] R. Berthet, A. Zerroukhi, G. Brun, T. Zecheru, C. Cincu, *Rev. Roum. Chim.* **2007**, *52*, 471.
[77] J. Robert Lingle, D. W. Peckham, A. McCurdy, J. Kim, in *Specialty optical fibers handbook*, (Eds: A. Méndez, T.F. Morse), Academic Press, **2007**, Light-Guiding Fundamentals and Fiber Design.
[78] a) A. Stefani, W. Yuan, S. Andresen, O. Bang, presented at the 20th International Conference on Plastic Optical Fibers, POF, Bilbao, Spain **2011**; b) G. Grover, S. Zhu, I. C. Twilley, *Text. Res. J.* **1993**, *63*, 257.
[79] S. Podzimek, *J. Appl. Polym. Sci.* **2014**, *131*.
[80] H.-J. Eichler, in *Lehrbuch der experimentalphysik, band 3 - optik*, (Eds: Bergmann, Schäfer), Walter de Gruyter, Berlin, New York **2004**.

[81] R. Klein, *Laser welding of plastics*, Wiley-VCH Verlag GmbH & Co. KGaA., Weinheim, Germany **2011**.
[82] a) J. Hao, M. Jayachandran, P. L. Kng, S. F. Foo, P. W. Aung Aung, Z. Cai, *Front. Optoelectron.* **2010**, *3*, 78; b) G. Wehrle, P. Nohama, H. J. Kalinowski, P. I. Torres, L. C. G. Valente, *Meas. Sci. Technol.* **2001**, *12*, 805; c) J. Schiefer, *Long term vital parameter monitoring (lavimo),* RWTH Aachen University/ ClinicalTrials.gov - U.S. National Institutes of Health, http://clinicaltrials.gov/show/NCT01626274, **2013** accessed *October, 2013*; d) A. Van Brakel, P. L. Swart, A. A. Chtcherbakov, M. G. Shlyagin, presented at the Advanced Sensor Systems and Applications II, Beijing, China **2004**; e) H. B. Liu, H. Y. Liu, G. D. Peng, P. L. Chu, *Opt. Commun.* **2003**, *219*, 139; f) J. Witt, F. Narbonneau, M. Schukar, K. Krebber, J. De Jonckheere, M. Jeanne, D. Kinet, B. Paquet, A. Depré, L. T. D'Angelo, T. Thiel, R. Logier, in *Fourth European Workshop on Optical Fibre Sensors* (Eds: J.L. Santos, B. Culshaw, J.M. López-Higuera, W.N. MacPherson), Porto, Portugal **2010**; g) F. Narbonneau, J. De Jonckheere, M. Jeanne, D. Kinet, J. Witt, K. Krebber, B. Paquet, A. Depré, L. T. D'Angelo, T. Thiel, R. Logier, in *Biophotonics: Photonic Solutions for Better Health Care II* (Eds: J. Popp, W. Drexler, V.V. Tuchin, D.L. Matthews), Brussels, Belgium **2010**; h) D. Kokkinos, S. Dehipawala, T. Holden, E. Cheung, M. Musa, G. Tremberger Jr, P. Schneider, D. Lieberman, T. Cheung, presented at the Optical Fibers and Sensors for Medical Diagnostics and Treatment Applications XII, San Francisco, CA, USA **2012**; i) M. Krehel, M. Schmid, R. Rossi, L. F. Boesel, G.-L. Bona, L. Scherer, *Sensors* **2014**, *14*, 13088.
[83] M. Krehel, M. Wolf, L. F. Boesel, R. M. Rossi, G.-L. Bona, L. J. Scherer, *Biomedical Optics Express* **2014**, *5*, 2537.
[84] a) K. M. Moerman, A. M. J. Sprengers, A. J. Nederveen, C. K. Simms, *Med. Eng. Phys.* **2013**, *35*, 486; b) A. V. Koulaxouzidis, V. C. Roberts, M. J. Holmes, V. A. Handerek, presented at the Applications of Optical Fiber Sensor, Glasgow, UK **2000**; c) T. L. Yeo, T. Sun, K. T. V. Grattan, D. Parry, R. Lade, B. D. Powell, *Sens. Actuators, B* **2005**, *110*, 148; d) K. Ni, C. C. Chan, X. Dong, L. Li, *Opt. Fiber Technol.* **2013**, *19*, 410; e) T. K. Lim, S. C. Tjin, L. G. Tay, C. H. Chua, Y. Wang, J. Brownjohn, in *Smart Structures and Devices* (Eds: D.K. Sood, R.A. Lawes, V.V. Varadan), Melbourne, VIC; Australia **2001**; f) N. Pleros, G. T. Kanellos, G. Papaioannou, presented at the 9th International Conference on Information Technology and Applications in Biomedicine, ITAB 2009, Larnaca; Cyprus **2009**; g) W. C. Wang, W. R. Ledoux, B. J. Sangeorzan, P. G. Reinhall, *J. Rehabil. Res. Dev.* **2005**, *42*, 315; h) R. P. Rocha, A. F. Silva, J. P. Carmo, J. H. Correia, *IEEE Eng. Med. Biol.* **2011**, *2011*, 458.
[85] T. L. Yeo, T. Sun, K. T. V. Grattan, *Sens. Actuators, A* **2008**, *144*, 280.
[86] M. Folke, L. Cernerud, M. Ekström, B. Hök, *Med. Biol. Eng. Comput.* **2003**, *41*, 377.
[87] M. Conde Pastor, F. Javier Menéndez, M. T. Sanz, E. Vila Abad, *Applied Psychophysiology Biofeedback* **2008**, *33*, 49.
[88] K. Doi, T. Ishizu, T. Fujita, E. Noiri, *Clin. Exp. Nephrol.* **2011**, *15*, 464.
[89] M. Nishyama, M. Miyamoto, K. Watanabe, *J. Biomed. Opt.* **2011**, *16*.
[90] D. J. Meredith, D. Clifton, P. Charlton, J. Brooks, C. W. Pugh, L. Tarassenko, *J. Med. Eng. Technol.* **2012**, *36*, 1.
[91] A. Grillet, D. Kinet, J. Witt, M. Schukar, K. Krebber, F. Pirotte, A. Depre, *IEEE Sens. J.* **2008**, *8*, 1215.
[92] a) C. Gaultier, R. Crapo, *Eur. Respir. J.* **1997**, *10*, 2913; b) D. Courteix, P. Obert, A. M. Lecoq, P. Guenon, G. Koch, *Eur. J. Appl. Physiol. Occup. Physiol.* **1997**, *76*, 264; c) S. J. Enright, V. B. Unnitham, C. Heward, L. Withnall, D. H. Davies, *Physical Therapy* **2006**, *86*, 345.
[93] E. Mitchell, S. Coyle, N. E. O'Connor, D. Diamond, T. Ward, presented at the International Conference on Body Sensor Networks, BSN 2010, Singapore, Singapore **2010**.
[94] S. Blanchard, J. D. Bronzino, in *Introduction to biomedical engineering (third edition)*, (Eds: J.D. Enderle, J.D. Bronzino), Academic Press, Boston **2012**.

[95] Z. B. Zhang, Y. H. Shen, W. D. Wang, B. Q. Wang, J. W. Zheng, *Journal of Medical and Biological Engineering* **2011**, *31*, 207.
[96] B. Venema, N. Blanik, V. Blazek, H. Gehring, A. Opp, S. Leonhardt, *IEEE Trans. Biomed. Eng.* **2012**, *59*, 2003.
[97] A. Schäfer, J. Vagedes, *Int. J. Cardiol.* **2013**, *166*, 15.
[98] P. Verdecchia, G. Schillaci, F. Boldrini, I. Zampi, C. Porcellati, *Hypertension* **1992**, *20*, 555.
[99] S. K. Gupta, S. H. Bodakhe, *Asian J. Pharm. Clin. Res.* **2013**, *6*, 5.
[100] D. Nair, S. Y. Tan, H. W. Gan, S. F. Lim, J. Tan, M. Zhu, H. Gao, N. H. Chua, W. L. Peh, K. H. Mak, *J Hum Hypertens* **2007**, *22*, 220.
[101] J. C. Ruiz-Rodriguez, A. Ruiz-Sanmartin, V. Ribas, J. Caballero, A. Garcia-Roche, J. Riera, X. Nuvials, M. de Nadal, O. de Sola-Morales, J. Serra, J. Rello, *Intensive Care Med.* **2013**, *39*.
[102] J. P. Isbister, *Transfusion Science* **1997**, *18*, 409.
[103] O. P. Habler, K. F. W. Messmer, *Transfusion Science* **1997**, *18*, 425.
[104] R. Boushel, C. A. Piantadosi, *Acta Physiol. Scand.* **2000**, *168*, 615.
[105] D. A. Hampton, M. A. Schreiber, *Transfusion* **2013**, *53 Suppl 1*, 52S.
[106] R. Araki, I. Nashimoto, in *Time-Resolved Spectroscopy and Imaging of Tissues* (Eds: B. Chance), Los Angeles, CA, USA **1991**.
[107] G. J. Kost, N. K. Tran, *Crit. Care Med.* **2011**, *39*, 2369.
[108] S. J. Barker, J. Curry, D. Redford, S. Morgan, *Anesthesiology* **2006**, *105*, 892.
[109] D. Kashyap, N. Chu, A. Apte, B. Wang, H. Liu, in *Optical Tomography and Spectroscopy of Tissue VII* (Eds: B. Chance, R.R. Alfano, B.J. Tromberg, M. Tamura, E.M. Sevick-Muraca), San Jose, CA, USA **2007**.
[110] Q. Liu, T. Vo-Dinh, *Medical Physics* **2009**, *36*, 4819.
[111] R. Aissaoui, C. Kauffmann, J. Dansereau, J. A. de Guise, *Med. Eng. Phys.* **2001**, *23*, 359.
[112] a) J. Kottner, A. Gefen, N. Lahmann, *International Journal of Nursing Studies* **2011**, *48*, 1339; b) J. Anders, A. Heinemann, C. Leffmann, M. Leutenegger, F. Profener, W. von Renteln-Kruse, *Deutsches Arzteblatt International* **2010**, *107*, 371.
[113] a) L. M. Rappl, *International Wound Journal* **2008**, *5*, 435; b) M. K. Henzel, K. M. Bogie, M. Guihan, C. H. Ho, *J. Rehabil. Res. Dev.* **2011**, *48*, XI.
[114] M. Rothmaier, M. P. Luong, F. Clemens, *Sensors* **2008**, *8*, 4318.
[115] A. Levi, M. Piovanelli, S. Furlan, B. Mazzolai, L. Beccai, *Sensors (Switzerland)* **2013**, *13*, 6578.
[116] J. M. Yuan, M. A. El-Sherif, S. Khalil, J. Fairneny, in *Industrial and Highway Sensors Technology* (Eds: B. Culshaw, M.A. Marcus, J.P. Dakin, S.D. Crossley, H.E. Knee), Providence, RI, USA **2003**.
[117] C. Yan, E. Ferraris, D. Reynaerts, *Procedia Eng.* **2011**, *25*, 495.
[118] B. M. Cowie, D. J. Webb, B. Tam, P. Slack, P. N. Brett, in (Eds), **2006**.
[119] E. Al-Fakih, N. Osman, A. Eshraghi, F. Adikan, *Sensors* **2013**, *13*, 10348.
[120] *Biomerge,* Bioimerosin Laboratories SA, Thessaloniki, Greece, http://www.bio-merge.com/flash.swf **2013** accessed *October, 2013*.
[121] J. E. Nelson, D. E. Treaster, W. S. Marras, *Clin. Biomech.* **2000**, *15*, 489.
[122] a) N. Noury, P. Rumeau, A. K. Bourke, G. ÓLaighin, J. E. Lundy, *IRBM* **2008**, *29*, 340; b) A. K. Bourke, J. V. O'Brien, G. M. Lyons, *Gait Posture* **2007**, *26*, 194.
[123] N. Vuillerme, N. Pinsault, O. Chenu, A. Fleury, Y. Payan, J. Demongeot, *Perv. and Mob. Comp.* **2009**, *5*, 268.
[124] *Temperature measurement- part 2: Expansion thermometers, BS1041-2.1:1985* **1985.**
[125] H. Chi, X. M. Tao, D. X. Yang, K. S. Chen, *Opt. Lett.* **2001**, *26*, 1949.

[126] S. Coyle, F. Benito-Lopez, R. Byrne, D. Diamond, in, 75 LNEE (Eds: A. Lay-Ekuakille, S.C. Mukhopadhyay), **2010**.
[127] D. Morris, S. Coyle, Y. Wu, K. T. Lau, G. Wallace, D. Diamond, *Sensors Actuators B: Chem.* **2009**, *139*, 231.
[128] L. Athanasekos, S. Pispas, C. Riziotis, in *Microstructured and Specialty Optical Fibres* (Eds: K. Kalli, A. Mendez), Brussels **2012**.
[129] P. Dumais, C. Callender, J. Jiang, C. Blanchetière, D. Celo, S. Jacob, C. Ledderhof, in *Photonics North 2011* (Eds), Ottawa, ON **2011**.
[130] K. Peters, *Smart Mater. Struct.* **2011**, *20*.
[131] Y.-Z. Su, M.-W. Hung, K.-C. Huang, *Phys. Procedia* **2011**, *19*, 379.
[132] Z. Xie, J. Tao, Y. Lu, K. Lin, J. Yan, P. Wang, H. Ming, *Opt. Commun.* **2009**, *282*, 439.
[133] A. Yarai, *Procedia Eng.* **2010**, *5*, 1180.
[134] M. A. El-Sherif, J. M. Yuan, A. MacDiarmid, *J. Intell. Mater. Syst. Struct.* **2000**, *11*, 407.
[135] B. Lee, S. Roh, J. Park, *Opt. Fiber Technol.* **2009**, *15*, 209.
[136] L. Wang, J. Ren, X. Han, T. Claes, X. Jian, P. Bienstman, R. Baets, M. Zhao, G. Morthier, *IEEE Photon. J.* **2012**, *4*, 920.
[137] P. Kozma, F. Kehl, E. Ehrentreich-Förster, C. Stamm, F. F. Bier, *Biosens. Bioelectron.* **2014**, *58*, 287.
[138] A. Leung, P. M. Shankar, R. Mutharasan, *Sens. Actuators, B* **2007**, *125*, 688.
[139] D. F. Merchant, P. J. Scully, N. F. Schmitt, *Sens. Actuators, A* **1999**, *76*, 365.
[140] H. A. Rahman, S. W. Harun, M. Yasin, S. W. Phang, S. S. A. Damanhuri, H. Arof, H. Ahmad, *Sens. Actuators, A* **2011**, *171*, 219.
[141] M. I. Zibaii, A. Kazemi, H. Latifi, M. K. Azar, S. M. Hosseini, M. H. Ghezelaiagh, *J. Photochem. Photobiol., B* **2010**, *101*, 313.
[142] C. Beres, F. V. B. de Nazaré, N. C. C. de Souza, M. A. L. Miguel, M. M. Werneck, *Biosens. Bioelectron.* **2011**, *30*, 328.
[143] S. Coyle, K. T. Lau, N. Moyna, D. O'Gorman, D. Diamond, F. Di Francesco, D. Costanzo, P. Salvo, M. G. Trivella, D. E. De Rossi, N. Taccini, R. Paradiso, J. A. Porchet, A. Ridolfi, J. Luprano, C. Chuzel, T. Lanier, F. Revol-Cavalier, S. Schoumacker, V. Mourier, I. Chartier, R. Convert, H. De-Moncuit, C. Bini, *IEEE Transactions on Information Technology in Biomedicine* **2010**, *14*, 364.
[144] S. Coyle, D. Morris, K. T. Lau, D. Diamond, N. Moyna, presented at the 6th International Workshop on Wearable and Implantable Body Sensor Networks, BSN 2009, Berkeley, CA, USA **2009**.
[145] G. Krupincová, M. Meloun, *J. Text. Inst.* **2013**, *104*, 1312.
[146] a) B. Selm, E. A. Gurel, M. Rothmaier, R. M. Rossi, L. J. Scherer, *J. Intell. Mater. Syst. Struct.* **2010**, *21*, 1061; b) J. C. Wang, B. H. Huang, B. Yang, *Text. Res. J.* **2013**, *83*, 1170.
[147] C. Zysset, T. W. Kinkeldei, N. Munzenrieder, K. Cherenack, G. Troster, *Ieee Transactions on Components Packaging and Manufacturing Technology* **2012**, *2*, 1107.
[148] a) T. Vervust, F. Bossuyt, F. Axisa, J. Vanfleteren, in (Eds), San Francisco, CA **2010**; b) K. Cherenack, L. van Pieterson, *J. Appl. Phys.* **2012**, *112*; c) L. Li, W. M. Au, Y. Li, K. M. Wan, W. Y. Chung, K. S. Wong, *Text. Res. J.* **2009**, *79*, 1670.
[149] A. Masuda, T. Murakami, K. Honda, S. Yamaguchi, *Journal of Textile Engineering* **2006**, *52*, 93.
[150] M. Rothmaier, B. Selm, S. Spichtig, D. Haensse, M. Wolf, *Opt. Express* **2008**, *16*, 12973.
[151] S. Mordon, C. Cochrane, J. C. Lesage, V. Koncar, presented at the 13th International Photodynamic Association World Congress, Bologna, Italy **2011**.
[152] C. Cochrane, S. R. Mordon, J. C. Lesage, V. Koncar, *Mater. Sci. Eng., C* **2013**, *33*, 1170.

[153] L. Ashok Kumar, C. Vigneswaran, T. Ramachandran, *J. Ind. Text.* **2010**, *39*, 305.
[154] J. Rantala, J. Hannikainen, J. Vanhala, *Pers. Ubiquit. Comput.* **2011**, *15*, 85.
[155] B. Selm, M. Rothmaier, M. Camenzind, T. Khan, H. Walt, *BIOMEDO* **2007**, *12*.
[156] J. P. Carmo, A. M. F. Da Silva, R. P. Rocha, J. H. Correia, *IEEE Sens. J.* **2012**, *12*, 261.
[157] A. F. Da Silva, A. F. Gonçalves, P. M. Mendes, J. H. Correia, *IEEE Sens. J.* **2011**, *11*, 2442.
[158] M. Rosenberger, S. Hessler, S. Belle, B. Schmauss, R. Hellmann, *Opt. Express* **2014**, *22*, 5483.
[159] a) A. F. Silva, F. Gonçalves, L. A. Ferreira, F. M. Araujo, N. S. Dias, J. P. Carmo, P. M. Mendes, J. H. Correia, presented at the 35th Annual Conference of the IEEE Industrial Electronics Society, IECON 2009, Porto, Portugal **2009**; b) A. F. Silva, F. Gonçalves, L. A. Ferreira, F. M. Araújo, P. M. Mendes, J. H. Correia, presented at the 5th International Materials Symposium MATERIAiS 2009 - 14th meeting of SPM - Sociedade Portuguesa de Materiais, Lisbon; Portugal **2010**.
[160] G. T. Kanellos, G. Papaioannou, D. Tsiokos, C. Mitrogiannis, G. Nianios, N. Pleros, *Opt. Express* **2010**, *18*, 179.
[161] R. K. Kramer, C. Majidi, R. Sahai, R. J. Wood, presented at the IEEE/RSJ International Conference on Intelligent Robots and Systems: Celebrating 50 Years of Robotics, IROS'11, San Francisco, CA, USA **2011**.
[162] S. Law, G. Barton, M. van Eijkelenborg, C. Yan, R. Lwin, J. Gan, in *Novel Optical Systems Design and Optimization IX* (Eds: J.M. Sasian, M.G. Turner), San Diego, CA, USA **2006**.
[163] R. Carta, P. Jourand, B. Hermans, J. Thone, D. Brosteaux, T. Vervust, F. Bossuyt, F. Axisa, J. Vanfleteren, R. Puers, *Sens. Actuators, A* **2009**, *156*, 79.
[164] a) X. Zhu, W. Chen, T. Nemoto, Y. Kanemitsu, K. I. Kitamura, K. I. Yamakoshi, presented at the 27th Annual International Conference of the Engineering in Medicine and Biology Society, IEEE-EMBS 2005, Shanghai; China **2005**; b) S. Akdemir Akar, S. Kara, F. Latifoğlu, V. Bilgiç, *Biomedical Signal Processing and Control* **2013**, *8*, 16.
[165] A. A. Stolov, B. E. Slyman, D. T. Burgess, A. S. Hokansson, J. Li, R. S. Allen, presented at the Optical Fibers and Sensors for Medical Diagnostics and Treatment Applications XIII, San Francisco, CA **2013**.
[166] F. Song, J. Xiao, A. J. Xie, S. W. Seo, *J. Opt.* **2014**, *16*.

List of figures

Brit Maike Quandt has received her B.Sc. and M.Sc. degree in Materials Science from ETH Zurich, Switzerland. Currently, she is a Ph.D. student in Electrical Engineering at ETH Zurich, based at Empa St. Gallen in the Department of Protection and Physiology. Her research focus lies on optical fiber textiles in the scope of creating wearable medical sensing setups.

Luciano Fernandes Boesel obtained his PhD in Materials Science and Technology from the Univ. of Minho (Portugal) in 2006. He then worked several years with biomaterials and biopolymers (hydrogels, biodegradable polymers) and joined Empa as a Scientist in 2010. Since 2014 he leads the group “Medical Textiles”, where his main focus are on the non-invasive body monitoring with optical fibers or fluorescent textiles and development of responsive transdermal delivery systems.

Rene M Rossi is physicist and obtained his PhD at ETH Zurich in the field of the complex man-clothing-environment interactions in a firefighting environment. Since 2003, he is the head of the Laboratory for Protection and Physiology at Empa, a group of 40 persons working in the field of high-tech fibres and textiles for near-to-body applications. One of the key topics of the laboratory are the development of textile-based sensors for medical applications.

Table of contents entry:

This review deals with possibilities in healthcare monitoring by means of optical fiber sensing. Fundamentals of optics and different optical fiber sensing techniques are discussed followed by a materials section and the various available non-invasive applications in which optical fibers can be used. The last section includes approaches for textile integration to allow for wearable long-term monitoring systems.

fiber optic sensors, wearable systems, healthcare monitoring, smart textiles, long-term monitoring

Keywords: fiber optic sensors, wearable systems, healthcare monitoring, smart textiles, long-term monitoring

Brit M. Quandt, Lukas J. Scherer, Luciano F. Boesel*, Martin Wolf, Gian-Luca Bona, René M. Rossi

Body-Monitoring and Health Supervision by means of Optical Fiber-Based Sensing Systems in Medical Textiles